1971

Matrix isolation studies of small molecules

Jacob Pacansky Jr.
Iowa State University

Matrix isolation studies of small molecules

by

Jacob Pacansky, Jr.

A Dissertation Submitted to the

Graduate Faculty in Partial Fulfillment of

The Requirements for the Degree of

DOCTOR OF PHILOSOPHY

Major Subject: Physical Chemistry

Approved:

Signature was redacted for privacy.

In Charge of Major Work

Signature was redacted for privacy.

For the Major Department

Signature was redacted for privacy.

For the Graduate College

Iowa State University
Of Science and Technology
Ames, Iowa

1971

TABLE OF CONTENTS

I. INTRODUCTION

This study of the infrared matrix isolation spectra of small molecules consists of two major sections. The first section is the infrared matrix isolation spectra of H_2S and D_2S performed under the usual assumptions of matrix isolation. These are: the potential field and the anharmonicity of the vibrations for the matrix isolated molecule are identical to those in the gas phase; and differences in isotopic shifts between the gas phase and the matrix are negligible. In the second section the validity of the assumptions is examined. HCN was chosen for this task because it is well characterized spectroscopically and its geometry is simple.

Initially, a simple perturbation treatment for the calculation of vibrational frequencies is developed and examples are given to illustrate the method. This approximation allows one to write simple separate expressions for each vibrational frequency and is valid for molecules whose terminal atoms are light compared to the central atoms. It is shown that for H_2S and D_2S the approximation is excellent and allows one to determine the factors which govern the relative vibrational frequency of ν_1, the symmetric stretching frequency and ν_3, the asymmetric stretching frequency.

All of the fundamentals of H_2S and D_2S were observed in argon and krypton matrices. The band centers, anharmonicities and force constants were calculated and reported. A large anomaly in the isotopic shift in the gas and matrix was observed. This violated one of the assumptions previously made.

All of the fundamentals were observed for $H^{12}C^{14}N$, $H^{13}C^{14}N$, $H^{12}C^{15}N$, $D^{12}C^{14}N$, $D^{13}C^{14}N$ and $D^{12}C^{15}N$ except ν_1 the CN stretch, for the hydrogen isotopes. Again a large discrepancy in the isotopic shifts in the gas and

matrix was observed. This anomaly was the greatest for hydrogen to deuterium isotopic substitution and decreased as the mass difference between the isotopes became smaller.

The assumption of the transferability of gas phase anharmonicities to the matrix frequencies was tested on the basis of a linear XYZ model. It was shown that for HCN there are negligible differences in the gas phase and matrix anharmonicities.

In order to determine the geometry of HCN in an argon matrix the ratio $(r_{CN}/r_{CH})_{matrix}$, where r_{CN} and r_{CH} are the equilibrium bond lengths, was compared to the corresponding ratio in the gas phase. The numerical values for the matrix ratios calculated on the basis of a linear XYZ vibrational model were inconsistent and in poor agreement with the gas phase ratios. A theoretical model was constructed to examine the geometry change to be expected from matrix perturbations. This model consisted of an HCN molecule enclosed in a spherical cavity of argon atoms. The total potential was assumed to be equal to the sum of the Lennard-Jones potential for the hydrogen and nitrogen ends of the HCN molecule plus the harmonic oscillator potentials for the CN and CH bonds. The total potential was minimized for a particular cavity size with respect to the position of the hydrogen, carbon and nitrogen atoms. The minimum in the total potential was found at a cavity size of 3.8 angstroms. The calculation shows a negligible change in the geometry for HCN. Hence, the disparity in the $(r_{CN}/r_{CH})_{matrix}$ was not due to geometry changes but rather due to an incorrect vibrational model.

Another vibrational model for HCN in an argon matrix was used to explain the anomalous isotopic shifts. This model was an extended linear

model, depicted as M-H-C-N-M, where M is a mass contribution from the matrix. On the basis of the extended model the isotopic anomalies are shown to arise from a combined effect of a change in force constant multiplied by the difference in isotopic masses. Hence, large differences in isotopic masses, for example, hydrogen to deuterium, magnify the effect while small differences produce a smaller effect.

Expressions for the matrix shifts in terms of the extended model are derived. These expressions emphasize the interrelation of mass changes and intermolecular force constants on the matrix shift.

The gas phase band center for ν_2 of $H^{12}C^{15}N$ and relative intensities of $H^{12}C^{14}N$ and $H^{13}C^{14}N$ are reported in the appendices.

These studies show that matrix isolation structure determination should not be considered reliable unless the isotopic discrepancy is within experimental uncertainty. Otherwise, the anomalies which arise because of the use of a free molecule model will be attributed to geometry changes.

II. DETERMINATION OF FORCE CONSTANTS BY CRYOGENIC MATRIX ISOLATION INFRARED SPECTROSCOPY

A. General Relationships for Vibrational Frequencies

One of the important problems in the interpretation of infrared spectroscopy of polyatomic molecules is the determination of the potential energy. Usually, the potential energy, V, is expressed as a Taylor series. In internal coordinates then:

$$V = V_o + \sum \left(\partial V / \partial R_i \right)_o \Delta R_i + 1/2 \left(\sum \left(\partial^2 V / \partial R_i \, \partial R_j \right)_o \Delta R_i \, \Delta R_j \right) + \cdots \qquad \text{(II.A.1)}$$

where V_o is an arbitrary constant which can be neglected. By virtue of the fact that at equilibrium V is a minimum all first derivatives in the expansion are zero. In the harmonic oscillator approximation cubic and higher order terms in the expansion are neglected, hence:

$$V = 1/2 \left(\sum f_{ij} \Delta R_i \Delta R_j \right) \qquad \text{(II.A.2)}$$

where

$$f_{ij} = \left(\partial^2 V / \partial R_i \, \partial R_j \right)_o$$

are the quadratic force constants. Eq. II.A.2 is known as the general quadratic valence force field.

The vibrational kinetic energy is

$$T = 1/2 (\dot{\underline{R}}^t \tilde{G}^{-1} \dot{\underline{R}}) \qquad \text{(II.A.3)}$$

where $\underline{\dot{R}}^t$ is the transpose of $\underline{\dot{R}}$, $\underline{\dot{R}}$ is a column vector containing the time derivatives of the internal coordinates, and $\tilde{G}^{-1}$ is the inverse of the $\tilde{G}$ matrix as defined in the Wilson FG formalism (40). In Wilson's formalism, the $\tilde{F}$ matrix contains the quadratic force constants while the $\tilde{G}$ matrix contains the mass and geometry relations associated with the vibrational modes; consequently, the $\tilde{F}$ matrix is related to the potential energy and the $\tilde{G}$ is related to the kinetic energy of the vibrations.

To find the vibrational frequencies one solves the following eigenvalue problem:

$$\tilde{G}\tilde{F}\underline{L}^{(i)} = \lambda_i \underline{L}^{(i)} \qquad \text{(II.A.4)}$$

or the secular determinant:

$$| \tilde{G}\tilde{F} - \lambda_i \tilde{I} | = 0 \qquad \text{(II.A.5)}$$

The eigenvalue λ_i, is related to the vibrational frequency ω_i, in reciprocal centimeters, by the formula

$$\lambda_i = (4\pi^2 c^2 \omega_i^2)/N_a \qquad \text{(II.A.6)}$$

where c = the speed of light and N_a = Avogadro's number. The components of the eigenvectors $\underline{L}^{(i)}$ give the amplitudes of the coordinates which contribute to λ_i or ω_i. The normal coordinate of a vibration can be defined in terms of the eigenvectors by an equation of the form:

$$\underline{R} = \tilde{L}\underline{Q} \qquad \text{(II.A.7)}$$

Here $\underline{R}$ is a column vector of the internal coordinates, $\underline{Q}$ is a column vector of the normal coordinates and $\tilde{L}$ is a matrix containing the L in

rows. The inverse eigenvectors $(L^{-1})^i$ are used to transform from the internal coordinate space to the normal coordinate space:

$$\underline{Q} = (\widetilde{L^{-1}})\underline{R} \qquad \text{(II.A.8)}$$

and are found by solving the eigenvalue equation

$$\tilde{F}\tilde{G}(\underline{L}^{-1})^i = \lambda_i(\underline{L}^{-1})^i \qquad \text{(II.A.9)}$$

Once the normal coordinates are found from Eq. II.A.8 then both V and T are in the form:

$$V = 1/2\left(\sum_{i=1}^{3N-6} \lambda_i Q_i^2\right) \qquad \text{(II.A.10)}$$

$$T = 1/2\left(\sum_{i=1}^{3N-6} \dot{Q}_i^2\right) \qquad \text{(II.A.11)}$$

which expresses the fact that in normal coordinate space the vibrational motion consists of 3N-6 independent oscillations.

From Eq. II.A.9 it is seen that $\tilde{F}$ and $\tilde{G}$ must be known before one can find $\underline{Q}$ for a molecule. $\tilde{G}$ is generally known if the molecular geometry is known; however, $\tilde{F}$ must be determined from the observed spectra using Eq. II.A.5. Unfortunately, for a problem of n frequencies the characteristic polynomial of the secular determinant is of degree n, while there are n(n+1)/2 independent, unknown force constants in the $\tilde{F}$ matrix. Thus, n(n-1)/2 additional data must be found to determine all the force constants.

The force constants can be written explicitly as a function of the vibrational frequencies and eigenvectors. By rewriting Eq. II.A.9 in the form

$$\tilde{F}\tilde{G}(\underline{L}^{-1}) = \tilde{\Lambda}(\underline{L}^{-1}) \qquad \text{(II.A.12)}$$

where $\tilde{\Lambda}$ = a diagonal matrix of the n eigenvalues, λ_i, and (L^{-1}) = a matrix of the $(\underline{L}^{-1})^i$. Substitution of $(L^{-1})(L^{-1})^t = I$ into Eq. II.A.12 gives

$$\tilde{F}(L^{-1})(L^{-1})^t\tilde{G}(L^{-1}) = \tilde{\Lambda}(L^{-1}) \qquad \text{(II.A.13)}$$

By multiplying Eq. II.A.13 by $(L^{-1})^t$ and requiring the following normalization condition,

$$(L^{-1})^t\tilde{G}(L^{-1}) = \tilde{I} \qquad \text{(II.A.14)}$$

one obtains

$$(L^{-1})^t\tilde{F}(L^{-1}) = \tilde{\Lambda} \qquad \text{(II.A.15)}$$

or

$$\tilde{F} = (L^{-1})\tilde{\Lambda}(L^{-1})^t \qquad \text{(II.A.16)}$$

For a particular λ_n, Eq. II.A.15 upon expansion gives

$$\lambda_n = \sum_i \sum_j F_{ij} L_{in} L_{jn} \qquad \text{(II.A.15a)}$$

The n(n+1)/2 force constants can be determined from Eq. II.A.16. Hence a knowledge of all the $(\underline{L}^{-1})^i$ and λ_i yields the necessary equations to determine the force constants. These equations for n=2 are illustrated below

$$F_{11} = (L^{-1}_{11})^2\lambda_1 + (L^{-1}_{12})^2\lambda_2 \qquad \text{(II.A.17)}$$

$$F_{22} = (L_{21}^{-1})^2 \lambda_1 + (L_{22}^{-1})^2 \lambda_2 \qquad \text{(II.A.18)}$$

$$F_{12} = (L_{11}^{-1})(L_{21}^{-1}) \lambda_1 + (L_{22}^{-1})(L_{12}^{-1}) \lambda_2 \qquad \text{(II.A.19)}$$

The somber revelation of Eqs. II.A.17 to II.A.19 is that the unknown F_{ij} are functions of the L_{ij} which are also unknown. It is instructive to investigate the changes in λ, $\tilde{F}$, $\tilde{G}$ and $(\tilde{L}^{-1})$ or $(\tilde{L})$ on the secular determinant in terms of cofactors rather than the $\underline{L}$ vectors. This is particularly desirable for small molecules where the cofactors are simple.

Dennison [11] shows that the k^{th} eigenvalue, λ_k, can be written as

$$\lambda_k = (\sum_{rs} F_{rs} A_{rk} A_{sk})/(\sum_{rs} G_{rs}^{-1} A_{rk} A_{sk}) \qquad \text{(II.A.20)}$$

where A_{rk} = the t^{th} cofactor found by striking out the t^{th} row and is proportional to L_{rk}, the r^{th} component of the k^{th} eigenvector; F_{rs}, and G_{rs}^{-1} are the matrix elements of the $\tilde{F}$ and $(\tilde{G}^{-1})$ matrices.

The eigenvalues λ_k depend explicitly on the potential constants and implicitly through A_{rk}, A_{sk} which themselves are functions of F_{rs}. Hence, changes in λ_k produced by changes in F_{rs} are found by differentiation, thus yielding:

$$\delta\lambda_k = (\sum_{rs} A_{rk} A_{sk} \delta F_{rs})/(\sum_{rs} G_{rs}^{-1} A_{rk} A_{sk}) \qquad \text{(II.A.21)}$$

Consequently, first order changes in the potential constants produce first order changes in λ_k. Similarly, the changes in λ_k caused by isotopic substitution or geometry changes is

$$\delta\lambda_k = -\lambda_k (\sum_{rs} A_{rk} A_{sk} \delta G_{rs}^{-1})/(\sum_{rs} G_{rs}^{-1} A_{rk} A_{sk}) \qquad \text{(II.A.22)}$$

In consideration of the above equations for λ_k the following remarks can be made: first order changes in the potential constants will produce first order changes in the frequencies; first order changes in the potential constants will produce changes in the A_{rk}, or L_{rk} as well as in the frequencies; first order changes in the L_{rk} or the A_{rk} without a change of potential have no influence on frequencies, at least to first order. This is known as Rayleigh's Principle which can be stated by $\partial \lambda_i / \partial L_{ki} = 0$.

B. Calculation of Vibrational Frequencies using Perturbation Theory

Perturbation theory has been applied to vibrational problems in the past (27,13,5,6). The following is the approach given by Wilson (40,p.239):

If $H_{ij} = (FG)_{ij}$, then the expanded secular determinant is

$$\begin{vmatrix} H_{11} - \lambda & H_{12} & \cdot & \cdot & H_{1n} \\ H_{21} & H_{22} - \lambda & 0 & \cdot & 0 \\ \cdot & \cdot & \cdot & & \cdot \\ \cdot & \cdot & & \cdot & \cdot \\ H_{n1} & 0 & \cdot & & H_{nn} - \lambda \end{vmatrix} = 0$$

The first order approximation for the t^{th} eigenvalue is

$$\lambda_t = H_{tt} \qquad \text{(II.B.1)}$$

In Appendix A it is shown that the second order approximation for the t^{th} eigenvalue is

$$\lambda_t = H_{tt} - \sum_{t \neq t'} H_{tt'} H_{t't} / (H_{tt} - H_{t't'}) \qquad \text{(II.B.2)}$$

Applications of Eqs. I.B.1 and I.B.2 are given in subsequent sections.

C. The Calculation of Force Constants from Isotopic Shifts of Vibrational Frequencies

The method is based on the "uncoupled oscillator" approximation, (5,6,13,40) which has been treated formally and applied before; however, the full implications and utility of this approach have not been developed. The approximate analysis described here has a number of advantages:

1. The force constants can be calculated without carrying out numerically a complete normal coordinate analysis.

2. No a priori assumptions are made about the nature of the force field except that it is harmonic. In the examples presented later, however, a general valence force field is employed. (See Eq. II.A.2)

3. The error in the calculated force constant caused by neglecting anharmonicity can be predicted by inspection.

4. The force constants calculated from the approximate equations compare favorably with those determined from detailed normal coordinate analysis.

A suitable set of coordinates to express the potential and kinetic energy are symmetry coordinates. In these coordinates, the matrix $\widehat{H} = \widetilde{FG}$ will be in block form greatly facilitating the expansion of the secular determinant.

Using Eq. II.B.2 for isotopic pairs of the same symmetry, the difference in the eigenvalues can be written:

$$\lambda_i = H_{ii} - H'_{ii} - \sum_{j\neq i}^{N} [H_{ji}H_{ij}/(H_{ii} - H_{jj}) - H'_{ji}H'_{ij}/(H'_{ii} - H'_{jj})] \quad \text{(II.C.1)}$$

which often can be satisfactorily approximated by the first order terms. Thus for a 2 x 2 block one obtains the pair of solutions:

$$\lambda_1 - \lambda_1' = F_{11}(G_{11} - G'_{11}) + F_{12}(G_{12} - G'_{12}) \qquad \text{(II.C.2)}$$

$$\lambda_2 - \lambda_2' = F_{22}(G_{22} - G'_{22}) + F_{12}(G_{12} - G'_{12}) \qquad \text{(II.C.3)}$$

and similarly for a 3 x 3 block:

$$\lambda_1 - \lambda_1' = F_{11}(G_{11} - G'_{11}) + F_{12}(G_{21} - G'_{21}) + F_{13}(G_{31} - G'_{31}) \qquad \text{(II.C.4)}$$

$$\lambda_2 - \lambda_2' = F_{22}(G_{22} - G'_{22}) + F_{21}(G_{12} - G'_{12}) + F_{23}(G_{32} - G'_{32}) \qquad \text{(II.C.5)}$$

$$\lambda_3 - \lambda_3' = F_{33}(G_{33} - G'_{33}) + F_{31}(G_{13} - G'_{13}) + F_{32}(G_{23} - G'_{23}) \qquad \text{(II.C.6)}$$

Now the significant simplification is this: For isotopic species of the same symmetry, these <u>differences</u> in the $\tilde{G}$ matrix elements often are much simpler than the matrix elements themselves. This fact gives rise to some rather useful expressions relating the force constants to the differences in isotopic eigenvalues.

Several examples are now given to illustrate the simplicity and accuracy of the above equations.

1. <u>XY_2 molecules</u>

To take advantage of the symmetry of a bent, symmetric, triatomic molecule, it is convenient to transform to symmetry coordinates:

$$S_1 = (1/2)^{1/2}(\Delta r_1 + \Delta r_2) \qquad \text{(II.C.7)}$$

$$S_2 = \Delta\alpha \qquad \text{(II.C.8)}$$

$$S_3 = (1/2)^{1/2}(\Delta r_1 - \Delta r_2) \qquad \text{(II.C.9)}$$

The matrix elements for $\tilde{F}$, $\tilde{G}$, and $\tilde{H} = \tilde{FG}$ are 3 x 3 matrices whose elements are given in Appendix B.

The roots of the expanded secular determinant are then,

$$\lambda_3^\circ = H_{33} = F_{33}G_{33} = (f_r - f_{rr})[\mu_x(1 - \cos\alpha) + \mu_y] \qquad \text{(II.C.10)}$$

and the two solutions of the quadratic equation in λ°;

$$\lambda^{\circ 2} - \lambda^\circ(H_{11} + H_{22}) + (H_{11}H_{22} - H_{12}H_{21}) = 0 \qquad \text{(II.C.11)}$$

One can express the sum and product of the two roots of this equation by well-known theorems (40,p.214):

$$\lambda_1^\circ + \lambda_2^\circ = H_{11} + H_{22} \qquad \text{(II.C.12)}$$

$$\lambda_1^\circ \lambda_2^\circ = H_{11}H_{22} - H_{12}H_{21} \qquad \text{(II.C.13)}$$

but for our purposes it is preferable to obtain solutions by means of the quadratic formula:

$$\lambda = 1/2(H_{11} + H_{22}) \pm 1/2[(H_{11} + H_{22})^2 - 4(H_{11}H_{22} - H_{12}H_{21})]^{1/2} \qquad \text{(II.C.14)}$$

where the "+" root refers to the symmetric stretch λ_1°, and the "-" root refers to the bending mode, λ_2°. This equation can be rearranged in the form:

$$\begin{matrix}\lambda_1^\circ \\ \lambda_2^\circ\end{matrix} = 1/2(H_{11} + H_{22})$$

$$\begin{matrix}+ \\ - \end{matrix} 1/2(H_{11} - H_{22})[1 + 4H_{12}H_{21}/(H_{11} - H_{22})^2]^{1/2} \qquad \text{(II.C.15)}$$

and to the extent that the term $4H_{12}H_{21}/(H_{11} - H_{22})^2$ is negligible, and the two roots can be written:

$$\lambda_1^\circ = H_{11} = (f_r + f_{rr})[\mu_x(1 + \cos\alpha) + \mu_y] - 2f_{r\alpha}\mu_x \sin\alpha \qquad \text{(II.C.16)}$$

$$\lambda_2^\circ = H_{22} = 2f_\alpha[\mu_y + \mu_x(1 - \cos\alpha)] - 2f_{r\alpha}\mu_x \sin\alpha \qquad \text{(II.C.17)}$$

Of course, corrections to Eqs. II.C.16 and II.C.17 could be obtained by expanding the square root in an infinite series but for many cases these equations are quite satisfactory.

Comparison of Eqs. II.C.16 and II.C.17 with II.C.12 and II.C.13 shows that the sum of the roots is unaffected by this approximation and that the product of the roots differs from the exact result by the term $H_{12}H_{21}$.

The accuracy of Eqs. II.C.16 and II.C.17, that is, the validity of the uncoupled oscillator approximation, depends on the size of the term:

$$4H_{12}H_{21}/(H_{11} - H_{22})^2 \qquad \text{(II.C.18)}$$

compared to unity.

The error produced in the eigenvalue, $\Delta\lambda^\circ = \lambda^\circ_{exact} - \lambda^\circ_{approx}$ by neglecting this term is:

$$\begin{matrix}+\Delta\lambda_1^\circ \\ -\Delta\lambda_2^\circ\end{matrix} = H_{12}H_{21}/(H_{11} - H_{22})^2 \qquad \text{(II.C.19)}$$

Table II.C.1 shows the size of this term for a number of molecules representing a variety of masses and geometries.

It is evident from this table and also from a term by term analysis of the right-hand side of Eq. II.C.19 that the approximation will be good except when two conditions are simultaneously met:

1. The mass of the central atom is small.

2. The mass of the terminal atom is equal or greater than the mass of the central atom.

The failure of the approximation is evident for O_3, OF_2 and OCl_2. For H_2S on the other hand the approximation is excellent.

Although Eqs. II.C.10, II.C.16, and II.C.17 are the same as those obtained from a perturbation treatment of the secular determinant, previous treatments at this point have proceeded to apply the approximate equations numerically. It is more instructive to analyze the equations further in general terms, however. For example, when data is available on terminally and symmetrically substituted isotopic species, YXY and Y'XY', Eqs. II.C.10, II.C.16, and II.C.17 can be written:

$$(\lambda_3^\circ - \lambda_3^{\circ\prime}) = (f_r - f_{rr})(\mu_y - \mu_y') \qquad \text{(II.C.20)}$$

$$(\lambda_1^\circ - \lambda_1^{\circ\prime}) = (f_r + f_{rr})(\mu_y - \mu_y') \qquad \text{(II.C.21)}$$

$$\lambda_2^\circ - \lambda_2^{\circ\prime} = 2f_a(\mu_y - \mu_y') \qquad \text{(II.C.22)}$$

$$(\lambda_3^\circ - \lambda_3^{\circ\prime}) + (\lambda_1^\circ - \lambda_1^{\circ\prime}) = 2f_r(\mu_y - \mu_y') \qquad \text{(II.C.23)}$$

$$(\lambda_3^\circ - \lambda_3^{\circ\prime}) - (\lambda_1^\circ - \lambda_1^{\circ\prime}) = 2f_{rr}(\mu_y - \mu_y') \qquad \text{(II.C.24)}$$

These simple isotopic relations yield accurate estimates of the valence force constants f_r, f_{rr} and f_α which do not depend upon any knowledge of the molecular geometry. The accuracy of these estimates is demonstrated in Table II.C.2 for H_2O and SO_2 and in Table II.C.3 for H_2Se and D_2Se.

The factors that govern the relative frequency of the asymmetric and symmetric vibrations of a molecule is a problem of chemical interest. Unfortunately, there is no convenient way to make such a comparison in a symmetric triatomic molecule when the eigenvalues are expressed in the forms given by Eqs. II.C.10, II.C.12, and II.C.13. On the other hand, Eqs. II.C.10 and II.C.16 yield a rather illuminating expression for this frequency difference:

$$\lambda_3^\circ - \lambda_1^\circ = -2f_r\mu_x \cos\alpha - 2f_{rr}(\mu_x + \mu_y) + 2f_{r\alpha}\mu_x \sin\alpha \qquad \text{(II.C.25)}$$

For a linear molecule, this reduces to:

$$\lambda_3^\circ - \lambda_1^\circ = 2f_r\mu_x - 2f_{rr}(\mu_x + \mu_y) \qquad \text{(II.C.26)}$$

and the difference in the frequencies is dominated by the term $2f_r\mu_x$ unless $\mu_x \ll \mu_y$. Since f_r is typically 10 x f_{rr} in absolute magnitude, and the condition for frequency coincidence is $f_r/f_{rr} = 1 + \mu_y/\mu_x$, two conclusions can be drawn:

1. Only linear hydrides would be expected to have nearly equal values of the symmetric and asymmetric modes, and

2. if f_{rr} is negative, coincidence can never occur.

For very acute molecules, $\alpha = 90°$, the frequency difference is controlled by different factors:

$$\lambda_3^\circ - \lambda_1^\circ = 2f_{rr}(\mu_x + \mu_y) + 2f_{r\alpha}\mu_x \qquad \text{(II.C.27)}$$

In this case, the frequency difference will tend to be small because the constants f_{rr} and $f_{r\alpha}$ are usually small. This is in agreement with the empirical observation that near coincidence of the symmetric and asymmetric stretching modes is most common in molecules that have very acute apex angles, e.g., H_2S, H_2Se (17)or SrF_2 (8). For intermediate angles, the term $-2f_{r\alpha x}\cos\alpha$ becomes the dominant one in Eq. II.C.25, with the concomitant result that $\omega_3 > \omega_1$, as is usually observed.

Some interesting conclusions can be drawn by expansion of the second order perturbation correction. Let $\lambda_{t'}^{(2)}$ be the second order term for the t' vibration, then in terms of $\tilde{F}$, $\tilde{G}$ matrix elements

$$\lambda_{t'}^{(2)} = F_{12}^2 G_{11} G_{22}/(F_{11}G_{11} - F_{22}G_{22})$$
$$+ F_{12}G_{12}(F_{11}G_{11} + F_{22}G_{22})/(F_{11}G_{11} - F_{22}G_{22})$$
$$+ G_{12}^2 F_{11} F_{22}/(F_{11}G_{11} - F_{22}G_{22}) \qquad \text{(II.C.28)}$$

If the symmetry coordinates are approximate normal coordinates, then $\tilde{F}$ and $\tilde{G}$ are approximately diagonal. Therefore, $\lambda_{t'}^{(2)} \approx 0$, since $F_{12} \approx 0$ and $G_{12} \approx 0$, that is the vibrations are uncoupled. As F_{12} and/or G_{12} increase, $\lambda_{t'}^{(2)}$, the coupling of the vibrations increases. Searching for conditions which cause $\lambda_{t'}^{(2)}$ to be small, relative to the first order energy, one can determine if the symmetry coordinates are approximate normal coordinates.

Analysis of $\lambda_{t'}^{(2)}$, is obtained by writing Eq. II.C.28 as

$$\lambda_{t'}^{(2)} = A + B + C \qquad \text{(II.C.29)}$$

where

$$A = F_{12}^2 G_{11} G_{22} / (F_{11} G_{11} - F_{22} G_{22}) \qquad \text{(II.C.30)}$$

$$B = F_{12} G_{12} (F_{11} G_{11} + F_{22} G_{22}) / (F_{11} G_{11} - F_{22} G_{22}) \qquad \text{(II.C.31)}$$

$$C = G_{12}^2 F_{11} F_{22} / (F_{11} G_{11} - F_{22} G_{22}) \qquad \text{(II.C.32)}$$

Two cases arise. First, since $G_{12} < 0$, $A > 0$, $C > 0$, and $B < 0$ for bent XY_2 molecules a partial cancellation of A or C by B can occur. The second case is $F_{12} < 0$ where no cancellation occurs. Table II.C.7 shows $\lambda_{t'}^{(2)}$ and the terms A, B, C for various molecules. Partial cancellation of A by B occurs for molecules where $m_x > m_y$, whereas for molecules with $m_x \leq m_y$, B partially cancels C. For OF_2 and SCl_2, $F_{12} < 0$ and no partial cancellation occurs. In all instances where $F_{12} > 0$ the B term always cancels the largest term.

The SO_2 molecule can be described accurately by an uncoupled oscillator. This is difficult to understand in view of the unfavorable mass difference. Table II.C.7 shows that for SO_2 the term A is very small, but while the terms B and C are much larger they almost cancel each other. The result is a very small coupling of the vibrational modes of SO_2 due to a fortuitous cancellation in B and C.

Further insight into the coupling of the vibrational modes is obtained by plotting $\lambda_{t'}^{(2)}$, A, B and C as functions of the bond angle. Since, for bent XY_2 molecules, $G_{12} = -(2)^{1/2} \mu_x \mathrm{SIN}\alpha / r$, then as α approaches 180°, A and B approach zero. Fig. II.C.1 shows A, B and C as functions of the

bond angle from 90° to 180° for SO_2, where the term A is approximately $\lambda^{(2)}_{t'}$, for reasons stated above. Similar plots are obtained for other molecules where the uncoupled oscillator approximation holds.

Fig. II.C.2 is a plot of $\lambda^{(2)}_{t'}$, versus bond angle for OF_2 where the uncoupled oscillator approximation fails. The plot reflects the expected large coupling of the symmetric stretching and bending modes of OF_2, and the unexpected sensitivity of the coupling on the bond angle.

The sensitivity is shown by a complete reversal of the assignment of the vibrational modes by increasing the bond angle from 104° to 107°. Fig. II.C.3 shows the dependence of the terms A, B, C on bond angle.

The discontinuity in OF_2 occurs because the denominator in Eq. II.C.28 is approximately equal to the difference in the vibrational frequencies, which are nearly equal at the equilibrium bond angle. A small increase in the bond angle produces an equality of the vibrational frequencies, which causes $\lambda^{(2)}_{t'}$ to go to infinity.

2. XY_3 molecules

The utility of the approximation is also exemplified by a pyramidal molecule of C_{3v} symmetry. In all, there are six modes--$2A_1$ and 2E. The A_1 modes are the symmetric stretch ν_1 and deformation ν_2 and the E modes consist of two pairs of degenerate asymmetric stretches ν_3 and bends ν_4. Thus the secular determinant consists of two 2 x 2 blocks, each block involving a stretch and deformation. For the isotopic pairs XY_3 and XY'_3, Eqs. II.C.2 and II.C.3 give:

$$(\lambda_1 - \lambda'_1) = (f_r + 2f_{rr})(\mu_y - \mu'_y) \qquad \text{(II.C.33)}$$

$$(\lambda_3 - \lambda_3') = (f_r - f_{rr})(\mu_y - \mu_y') \qquad \text{(II.C.34)}$$

$$(\lambda_2 - \lambda_2') = (f_\alpha + 2f_{\alpha\alpha})(\mu_y - \mu_y')\left[\frac{2 + 4\cos\alpha}{1 + \cos\alpha}\right] \qquad \text{(II.C.35)}$$

$$(\lambda_4 - \lambda_4') = (f_\alpha + f_{\alpha\alpha})(\mu_y - \mu_y')\left[\frac{2 + \cos\alpha}{1 + \cos\alpha}\right] \qquad \text{(II.C.36)}$$

In these equations, α = the Y-X-Y bond angle, and μ_y = the reciprocal of the mass of atom Y. These simple expressions give surprisingly accurate values of the force constants compared to the more complicated expressions of the standard treatment (18,p.188). (See Table II.C.4)

3. XY_4 molecules

Results of similar accuracy are obtained for tetrahedral molecules. The nine vibrations are of symmetry A_1, E and 2F. Hence the symmetric stretch ν_1 and doubly degenerate bend ν_2 are identical to the exact treatment (1 x 1 blocks), while the asymmetric stretch ν_3 and the asymmetric bend ν_4 fall in a 2 x 2 block of the secular determinant. For terminally substituted pairs XY_4 and XY_4', the resultant equations for the eigenvalue differences are:

$$(\lambda_1 - \lambda_1') = (f_r + 3f_{rr})(\mu_y - \mu_y') \qquad \text{(II.C.37)}$$

$$(\lambda_2 - \lambda_2') = 3(f_\alpha - 2f_{\alpha\alpha} + f'_{\alpha\alpha})(\mu_y - \mu_y') \qquad \text{(II.C.38)}$$

$$(\lambda_3 - \lambda_3') = (f_r - f_{rr})(\mu_y - \mu_y') \qquad \text{(II.C.39)}$$

$$(\lambda_4 - \lambda_4') = 2(f_\alpha - f'_{\alpha\alpha})(\mu_y - \mu_y') \qquad \text{(II.C.40)}$$

In these equations the constant $f_{\alpha\alpha}$ = the angle-angle interaction constant between the two coordinates having a common bond and $f'_{\alpha\alpha}$ = the

interaction constant between nonadjacent angles. A comparison with the more detailed computation is shown in Table II.C.5.

4. XY_2Z_2 molecules

The tetrahedral XY_2Z_2 molecules offer a more challenging example. The nine vibrations are of symmetry $4A_1$, A_2, $2B_1$, and $2B_2$. The A_2, B_1 and B_2 vibrations of SiH_2Cl_2 and SiD_2Cl_2 were chosen to test the calculation. The description of the modes is as follows:

A_2 $\quad \nu_5$ H torsion

B_1 $\quad \nu_6$ Si-H stretch

$\quad \nu_7$ Si-H rock

B_2 $\quad \nu_8$ Si-Cl rock

$\quad \nu_9$ Si-Cl stretch

Eqs. II.C.2 and II.C.3 give:

$$(\lambda_5 - \lambda_5') = F_{55}[(3/2)(\mu_y - \mu_y')/r_{xy}^2] \qquad \text{(II.C.41)}$$

$$(\lambda_6 - \lambda_6') = F_{66}(\mu_y - \mu_y') \qquad \text{(II.C.42)}$$

$$(\lambda_7 - \lambda_7') = F_{77}[(1/2)(\mu_y - \mu_y')/r_{xy}^2] \qquad \text{(II.C.43)}$$

$$(\lambda_8 - \lambda_8') = F_{88}[(3/2)(\mu_y - \mu_y')/r_{xy}^2] \qquad \text{(II.C.44)}$$

$$(\lambda_9 - \lambda_9') = 0 \qquad \text{(II.C.45)}$$

The results are compared in Table II.C.6. It is interesting that the detailed normal coordinate analysis (10) leads to two possible sets of potential constants for SiH_2Cl_2 and that these approximate equations converge to the correct set. The zero isotope shift predicted for ν_9 is verified by the small observed shift--590 cm^{-1} for H_2SiCl_2 to 566 cm^{-1} for D_2SiCl_2.

The effect of neglecting anharmonicity in the force constant calculation can be estimated by assuming that the observed frequency ν and the harmonic frequency ω are related by an equation of the form:

$$\nu = \omega(1 - \alpha) \qquad \text{(II.C.46)}$$

It follows that:

$$\lambda_{obs} = \lambda_{harm}(1 - \alpha)^2 \qquad \text{(II.C.47)}$$

Since the inequality $\alpha > \alpha'$ is always true if the primed isotopic species is assigned to the heavier isotope, the isotopic difference of the eigenvalues obeys the inequality:

$$(\lambda_{obs} - \lambda'_{obs}) < (\lambda_{harm} - \lambda'_{harm}) \qquad \text{(II.C.48)}$$

Thus the use of observed frequencies in Eqs. II.C.2 to II.C.6 produces lower bounds to the true force constants, provided no other vibrational interactions are important.

Table II.C.1. The value of $|\Delta\lambda^{\circ}|$ for some typical triatomic molecules

Molecule	λ_1°	λ_2°	$\lvert\Delta\lambda^{\circ}\rvert$
H_2O[a]	8.65208	1.60104	0.00725
H_2S[b]	4.36491	0.86901	0.00001
H_2Se[b]	3.50370	0.65938	0.00290
SO_2[c]	0.80318	0.16317	0.00834
ClO_2[d]	0.54613	0.12218	0.03469
OF_2[d]	0.50846	0.12521	0.06028
O_3[d]	0.72589	0.29282	0.31287
OCl_2[d]	0.27887	0.06033	0.22657

[a]Source: (29).

[b]Source: (17).

[c]Source: (38).

[d]Source: (30).

Table II.C.2. Comparison of the force constants of H_2O and SO_2 calculated from Eqs. II.C.20 to II.C.24 with best gas phase values. All constants are in Millidynes/A

	H_2O[a]		
	Observed frequencies	Harmonic frequencies	Best values
f_r	7.603	8.467	8.451 ± .004
f_{rr}	-0.514	-0.090	-0.100 ± .004
f_α	0.680	0.750	0.759 ± .002
$f_{r\alpha}$	0.861	0.210	0.327 ± .025

	SO_2[b]		
	Observed frequencies	Harmonic frequencies	Best values[c]
f_r	9.71	10.33	10.29 ± 0.20
f_{rr}	0.03	0.08	0.04 ± 0.20
f_α	0.78	0.82	0.816 ± 0.007
$f_{r\alpha}$	0.17	0.24	0.25 ± 0.21

[a]Source: (29).

[b]Source: (1).

[c]Source: (36).

Table II.C.3. Harmonic valence force constants of H_2Se and D_2Se (m dyn/A)[a]

	Approximate Equations	Exact Equations
f_r	3.511	3.498
f_{rr}	-0.018	-0.021
f_α	0.328	0.342

[a]Source: (17).

Table II.C.4 Observed valence force constants[a] NH_3 and PH_3 (m dyn/A)

	NH_3		PH_3	
	Approximate equations	Exact equations	Approximate equations	Exact equations
f_r	6.278	6.541	3.008	3.096
f_{rr}	0.12	0.002	-0.006	-0.065
f_α	0.519	0.553	0.330	0.360
$f_{\alpha\alpha}$	-0.088	-0.068	-0.021	0.002

[a]Source: (12).

Table II.C.5. Harmonic valence force constants[a] of CH_4 and CD_4 (m dyn/A)

	Approximate equations	Exact equations
$f_r + 3f_{rr}$	5.843	5.842
$f_\alpha - 2f_{\alpha\alpha} + f_{\alpha\alpha'}$	0.486	0.486
$f_r - f_{rr}$	5.362	5.383
$f_\alpha - f_{\alpha\alpha'}$	0.469	0.458[b]

[a]Source: (12).

[b]There is a typographical error in Table III of reference (12) where this constant is tabulated as negative. This is inconsistent with their Fig. 1.

Table II.C.6. F matrix elements for SiH_2Cl_2 and SiD_2Cl_2 ($r_{xy} = r_{SiH} = 1.46A$)

	Approximate equations		Exact equations
F_{55}	0.43	m dynA/rad^2	0.42
F_{66}	2.76	m dyn/A	2.81
F_{77}	0.74	m dynA/rad^2	0.73
F_{88}	0.55	m dynA/rad^2	0.60
F_{99}	indeterminant		2.89
$(\lambda_9 - \lambda_9)$	0		0.02

[a]Source: (10).

Table II.C.7. The value of $\lambda_{t'}^{(2)}$ for some typical triatomic molecules

	$\lambda_{t'}^{(2)}$	A	B	C
H_2O	-0.00026	0.03455	-0.04141	0.00660
H_2S	0.00002	0.00514	-0.00614	0.00101
H_2Se	0.00000	0.00000	0.00000	0.00000
SO_2	0.00511	0.00200	-0.01613	0.01924
NO_2	0.03799	0.01390	-0.08867	0.11280
ClO_2	0.00121	0.00252	-0.01480	0.01349
O_3	0.07718	0.02182	-0.13381	0.18920
OF_2	2.37810	0.06965	0.67480	1.63400
OCl_2	-0.00492	0.02737	-0.10150	0.06921
SCl_2	0.02224	0.00046	0.00632	0.01546

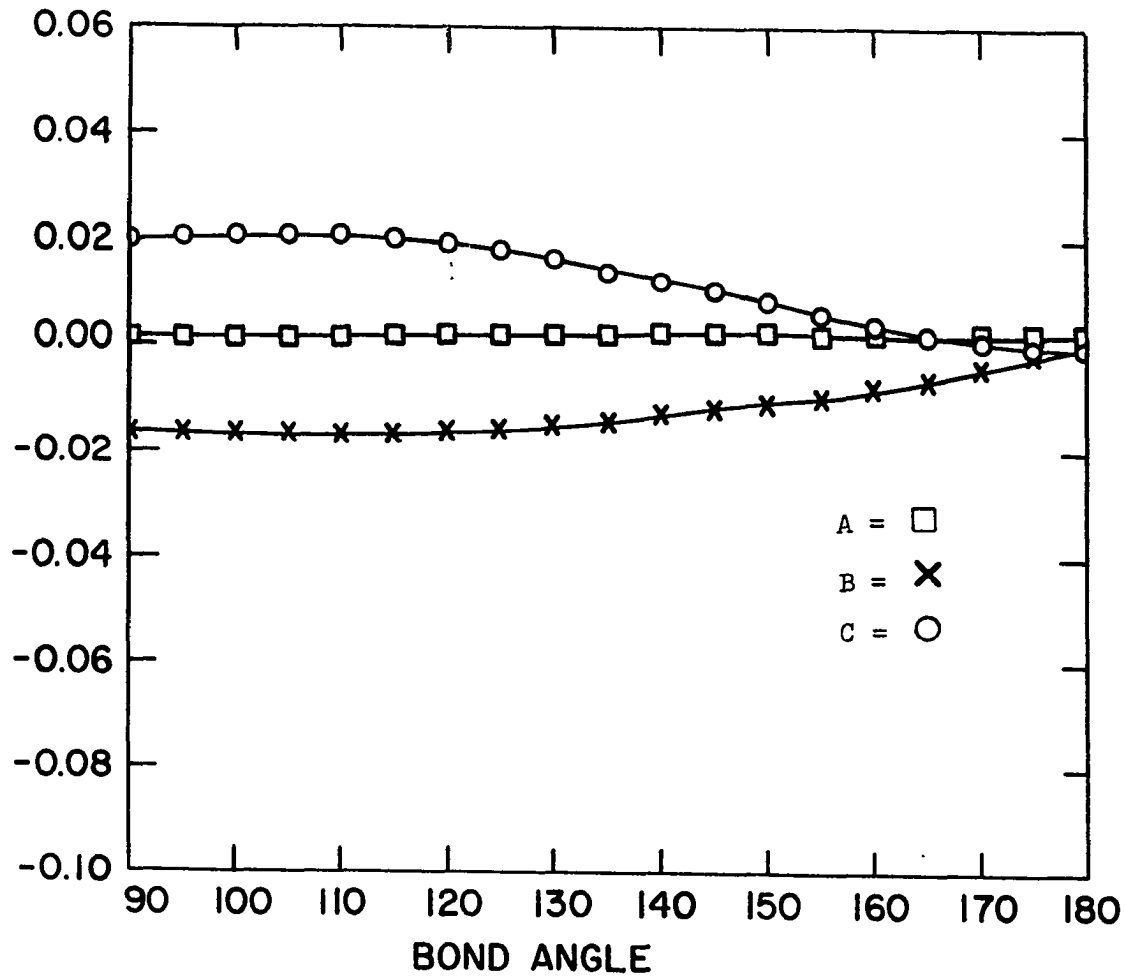

Fig. II.C.1. A plot of Eqs. II.C.30 to II.C.32 against the bond angle for SO_2

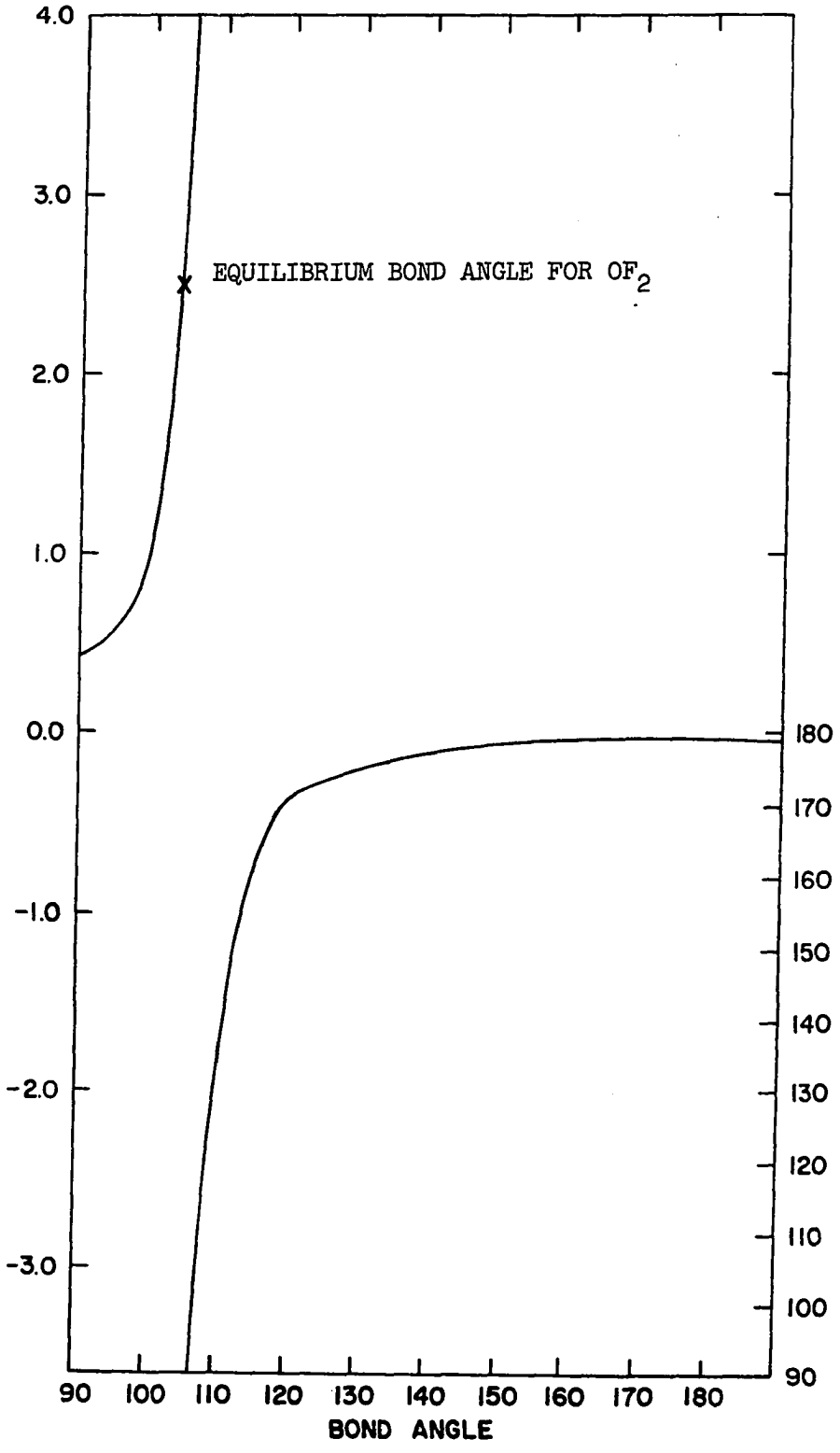

Fig. II.C.2. A plot of $\lambda_t^{(2)}$ against the bond angle for OF_2

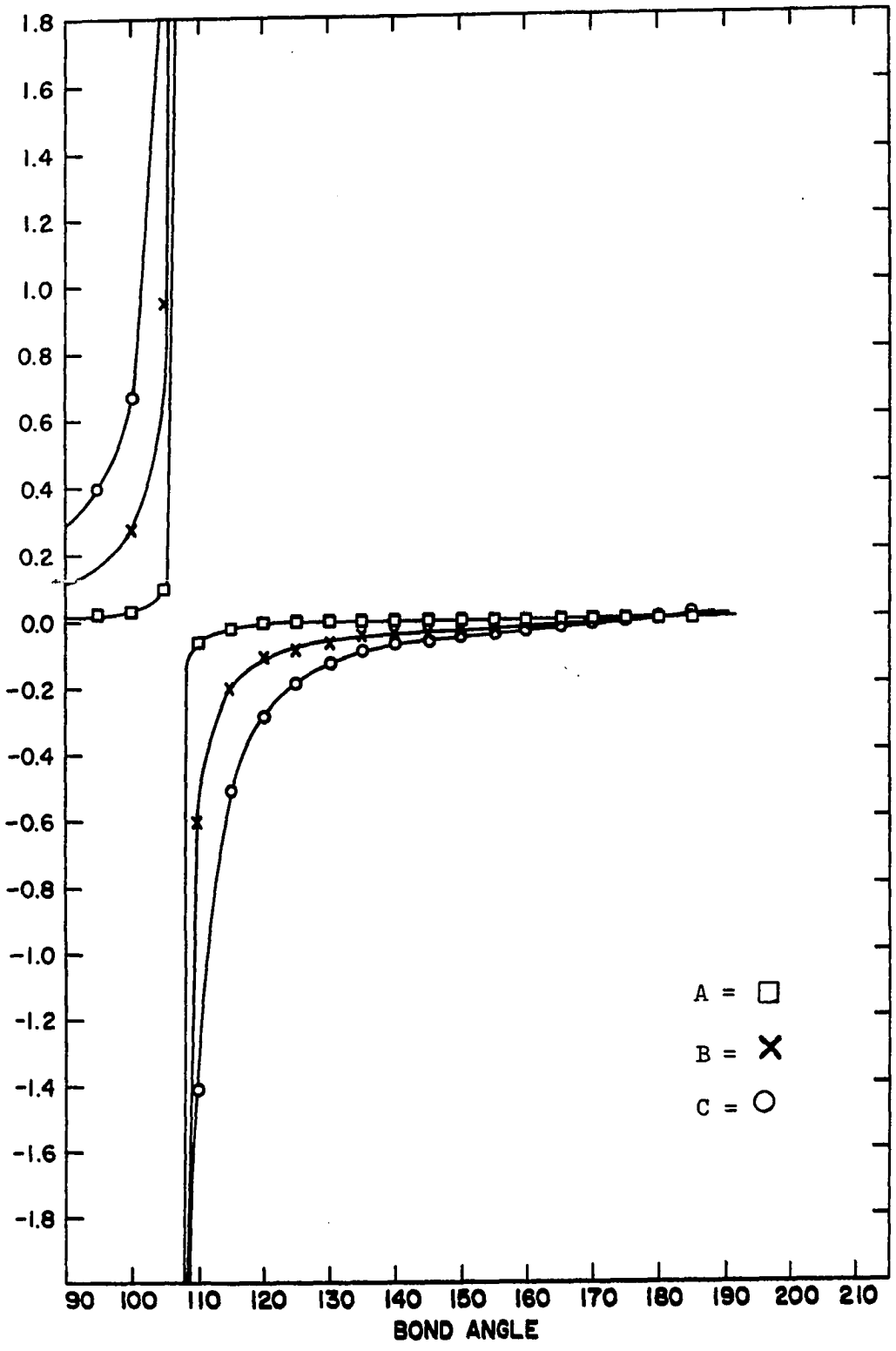

Fig. II.C.3. A plot of A,B,C against bond angle for OF_2

D. Matrix Isolation Spectroscopy: Assumptions

Infrared matrix isolation has been reviewed by several authors (4,22,32). The matrix isolation technique, involves the deposition of a dilute mixture of sample and rare gas onto a transparent window at liquid helium temperatures. Afterwards, the matrix is examined spectroscopically.

In comparison with the gas phase vibrational spectra where fundamental absorptions are accompanied by large rotational envelopes, the matrix spectra show only a sharp band, that of the fundamental vibrational absorption. However, due to small solvent shifts, band centers from matrix spectra do not coincide with those from gas phase spectra.

The great advantage of matrix isolation spectroscopy is the enhanced resolution. At liquid helium temperatures the absorptions bands are very narrow with half widths less than one cm^{-1} being common. Consequently, with high resolution instrumentation, bands due to isotopic species can be resolved.

Recently, Allavena, et al. (1) have investigated the matrix spectra of several isotopic species of SO_2 in Kr and Ar matrices under high resolution conditions. They concluded that the potential field and geometry of SO_2 was negligibly different from that obtained from gas phase measurements. The same conclusions were also drawn from other similar studies (8,24). These studies make the following assumptions:

1. The geometry of a gaseous species does not change upon isolation in a rare gas matrix.

2. Small solvent shifts can be neglected.

3. Differences in isotopic frequencies in the gas phase are identical

to differences in isotopic frequencies in rare gas matrices.

4. Gas phase band intensities are the same as band intensities in rare gas matrices.

Utilizing the above assumptions the matrix isolation spectrum of H_2S and D_2S has been studied (31) and is discussed in the next section.

E. Matrix Isolation of H_2S and D_2S in Argon and Krypton Matrices: An Example of an Uncoupled Oscillator

1. Introduction

The molecules H_2S and D_2S offer an excellent opportunity for demonstrating the application of matrix isolation spectroscopy, for despite the fact that the spectrum of H_2S and D_2S has been the object of extensive study (2,3,15,19,25,26,39) for many years, its interpretation is still incomplete. Indeed, the asymmetric stretching fundamental ν_3 has never been observed, even though this feature is commonly the most intense one in the vibration-rotation spectrum of triatomic molecules. The complexity of the spectrum arises from the near coincidence of the stretching frequencies, ν_1 and ν_3. Not only does the superposition of the rotational envelopes hinder the location of the origins, but the closeness of the frequencies also causes the overtone-combination levels (v_1,v_2,v_3) and (v_1-2,v_2,v_3+2) to interact strongly, thus complicating the overtone-combination analysis (39).

2. Experimental

All spectra were measured with a Perkin-Elmer E-13 monochromator. The frequencies were calibrated with NH_3, H_2O or HBr (33) depending on the

region under study, and the reported frequencies are the mean of at least two separate scans. The values reported are believed to be precise within $\pm$ 0.15 cm^{-1}.

Refrigeration was obtained with an Andonian variable temperature cryostat. The deposition window was mounted in a compression holder milled from OFHC copper. Indium wire and foil (purity stated by manufacturer to be 99.999%) were used to insure thermal contact betweeen the window and holder and between the holder and the cryostat block. Under operating conditions the temperature of the block was about 8°K. The window temperature was undoubtedly slightly higher.

The gas handling and vacuum systems were constructed of copper. The vacuum system consisted of a mechanical fore pump, oil diffusion pump, liquid nitrogen trap and appropriate bellows valves. The pressure was monitored at several points in the system with cold cathode sensors, and ambient pressure prior to liquid helium transfer was 10^{-6} torr. Samples were prepared using standard manometric techniques. The deposition rate was controlled with a Granville-Phillips standard leak and measured with a Wallace-Tiernan manometer. Deposition rates were typically 0.1 or 0.2 millimoles of matrix per minute. H_2S and D_2S were obtained commercially and used without further purification except that the samples were degassed at liquid nitrogen temperatures prior to dilution with the matrix gas. The krypton and argon were stated by the manufacturer to contain less than 105 ppm and 15 ppm impurities respectively.

Although no isotope exchange occurred in the vacuum system, some incompatibility between the vacuum system and the samples were encountered.

It was found that H_2S and D_2S was absorbed by, or reacted with, the copper and viton components of the system during deposition. When various efforts to "cure" the system proved fruitless an empirical approach was adopted. H_2S and D_2S were found to be stable in glass and stainless steel, so samples of sufficient concentration to produce sharp, polymer-free matrix spectra were prepared and stored in a glass bulb with a stainless steel valve. These samples (approximately one mole percent) were then deposited at a rate which experience with other molecules has shown to be adequate to insure isolation. This difficulty, of course, made it impossible to estimate the actual concentration of H_2S in the matrix.

3. Results

The matrix spectrum of H_2S in argon is shown in Fig. II.E.1. This spectrum is qualitatively the same as that of D_2S, and there is no substantial change in the features when krypton is used as a matrix. The spectrum of a 1:1 mixture of H_2S and D_2S was a superposition of the spectra of the pure isotopic species and showed no features attributable to HDS or any of the multiplets characteristic of dimers composed of mixed isotopic species. Controlled diffusion experiments showed no marked reversible temperature dependence and all the features assigned to monomeric H_2S disappeared irreversibly at the same rate. Figure II.E.2 shows a controlled diffusion experiment for ν_1 and ν_3 D_2S in krypton. The spectrum drawn with the light line is for the deposition at 12°K. The additional spectra were measured after diffusion at 40°K for ten minutes. All spectra were recorded at 12°K. The observed absorption frequencies of H_2S and D_2S are tabulated in Table II.E.1.

4. Discussion

The geometry of H_2S is well established (15), and the gas phase vibration-rotation spectrum has been examined extensively. Despite the presence of vibrational resonances in the overtone-combination bands, the vibrational levels seem to have been satisfactorily characterized, except for one disconcerting fact, the asymmetric stretch has never been observed for either H_2S (18) or D_2S (25). This is particularly surprising in view of the fact that this vibration is usually quite intense in the spectra of triatomic molecules. By subtraction of the combination frequencies:

$$\nu(0,1,1) - \nu(1,1,0) = \omega_3 - \omega_1 + 2(X_{33} - X_{11}) + 3/2(X_{23} - X_{12})$$

$$\approx \omega_3 - \omega_1 \qquad \text{(II.E.1)}$$

one would anticipate that the asymmetric stretching mode should lie about 10.1 cm^{-1} and 11.7 cm^{-1} above the symmetric mode in H_2S and D_2S respectively. Since these levels are unperturbed by the vibrational resonance, this estimate ought to be good, provided the anharmonic corrections $(X_{33} - X_{11})$ and $(X_{23} - X_{12})$ cancel one another. Published values of these constants indicate this cancellation is virtually exact, hence the band center of the ν_3 vibration in the gas phase should be located at 2626.14 cm^{-1} and 1909.13 cm^{-1} for H_2S and D_2S respectively.

The matrix spectra qualitatively support these estimates of the location of the band center of the ν_3 vibration. As seen in Table II.E.1, the position of the ν_3 band is approximately 10 cm^{-1} above the ν_1 band in both matrices, although the agreement is not exact since these fundamental frequencies are shifted by different amounts in the matrix. On the basis

of the matrix data alone one might presume that $\nu_3 < \nu_1$ but such an assignment is not consistent with the envelope shapes of the overtone-combination bands in the gas phase and is excluded on that basis.

The matrix spectrum has allowed a fairly unambiguous identification of ν_3 fundamental but it does not shed much light on the anomalous lack of intensity of this vibration in the gas phase. It has been general experience that the selection rules and relative intensity of vibrational transitions in the gas phase hold in the matrix, at least qualitatively. Since the ν_3 and ν_1 modes are of comparable intensity in the matrix but the ν_3 mode is apparently very weak in the gas, this experience appears to be violated in this case. At this point the weak intensity of the ν_3 vibration in the gas phase spectrum remains unexplained.

In this analysis, as in most vibrational treatments, it is presumed that the force field is harmonic. Thus, the force constants derived from Eqs. II.C.20 to II.C.24 using observed frequencies, will yield lower bounds to the harmonic frequencies.

These equations are now applied to H_2S. Since the geometry of H_2S is known ($\alpha = 92°07'$), the product rule for the ν_3 vibration can be used to estimate the anharmonic corrections if one assumes that the corrections for isotopic species are related by:

$$\alpha_i / \alpha_i' = \omega_i / \omega_i' \qquad \text{(II.E.2)}$$

Experimentally this relation seems especially valid for symmetric terminal isotopic pairs (1). In order to determine all six anharmonic corrections, an additional assumption is required. The gas phase data indicate that an appropriate one is $\alpha_1 = \alpha_3$. The anharmonic corrections

the harmonic frequencies, and eigenvalues based on this approximation are presented in Table II.E.2. The force constants f_r, f_{rr} and f_α are computed from Eqs. II.C.22 to II.C.24 and $f_{r\alpha}$ is calculated from an expression derived from Eqs. II.C.12, II.C.21 and II.C.22.

$$f_{r\alpha} = -[(\lambda_1^\circ + \lambda_2^\circ) - (\lambda_1^\circ - \lambda_1^{\circ\prime})(\mu_y + \mu_x(1 + \cos\alpha))/(\mu_y - \mu_y') - (\lambda_2^\circ - \lambda_2^{\circ\prime})(\mu_y + \mu_x(1 - \cos\alpha))/(\mu_y - \mu_y')]/4\mu_x \sin\alpha \quad \text{(II.E.3)}$$

The force constants calculated from the matrix and gas phase data are compared in Table II.E.3.

Table II.E.4 shows the observed matrix and gas phase isotopic shifts, where Δ_1, Δ_2, Δ_3 are the differences in the isotopic frequencies of ν_1, ν_2, and ν_3 for hydrogen to deuterium substitution. The matrix isotopic shifts are different than the gas phase isotopic shifts. This is disconcerting since infrared spectroscopists use isotopic shifts to determine molecular parameters in a variety of solvents assuming isotopic shifts are solvent independent.

The remainder of this thesis offers an explanation for this effect through the use of a simpler system--hydrogen cyanide and several of its isotopic species. In addition other fundamental assumptions of matrix isolation will also be studied in the next sections.

Table II.E.1. The observed vibrational frequencies of H_2S and D_2S in argon and krypton matrices

	Argon		Krypton	
	H_2S	D_2S	H_2S	D_2S
ν_1	2568.78	1862.10	2566.14	1860.49
ν_2	1179.54	853.17	1176.90	850.57
ν_3	2581.78	1870.33	2575.72	1866.50

Table II.E.2. Values of the anharmonic corrections, harmonic frequencies and eigenvalues of H_2S and D_2S

	Gas[a]	Ar	Kr
α_1	0.0394	0.0287	0.0297
α_2	0.0262	0.0332	0.0307
α_3	0.0387	0.0287	0.0297
α_1'	0.0283	0.0259	0.0213
α_2'	0.0188	0.0238	0.0220
α_3'	0.0278	0.0206	0.0213
ω_1	2721.92	2644.57	2644.60
ω_2	1214.51	1220.06	1214.21
ω_3	2733.36	2657.96	2654.48
ω_1'	1952.08	1901.25	1901.02
ω_2'	872.12	873.96	869.72
ω_3'	1963.88	1909.65	1907.16
λ_1°	4.36491	4.12036	4.12045
λ_2°	0.86901	0.87694	0.86858
λ_3°	4.40167	4.16218	4.15129
$\lambda_1^{\circ\prime}$	2.24502	2.12962	2.12911
$\lambda_2^{\circ\prime}$	0.44810	0.44999	0.44564
$\lambda_3^{\circ\prime}$	2.27224	2.14848	2.14288

[a]Source: (17).

Table II.E.3. Harmonic force constants of H_2S (millidynes/A)

	Ar	Kr	Gas[b]
f_r	4.040[a] ± 0.003	4.035[a] ± .003	4.286
f_{rr}	-0.023 ± .003	-0.017 ± .003	-0.011
f_α	0.431 ± .002	0.427 ± .002	0.426
$f_{r\alpha}$	-0.062 ± .004	-0.052 ± .004	0.066

[a]The uncertainties in the force constants represent only the result of error propagation.

[b]Source: (17).

Table II.E.4. Observed matrix and gas phase isotopic shifts

		Argon	Krypton	Gas
	H_2S	2581.8	2575.7	2628.5[a]
ν_3	Δ_3	711.5	709.2	717.1
	D_2S	1870.3	1866.5	1909.1
	H_2S	2568.8	2566.1	2614.4[a]
ν_1	Δ_1	706.7	705.6	718.2
	D_2S	1862.1	1860.5	1896.4
	H_2S	1179.5	1176.9	1182.7
ν_2	Δ_2	326.3	326.3	327.2
	D_2S	853.2	850.6	855.5

[a]Source: (14).

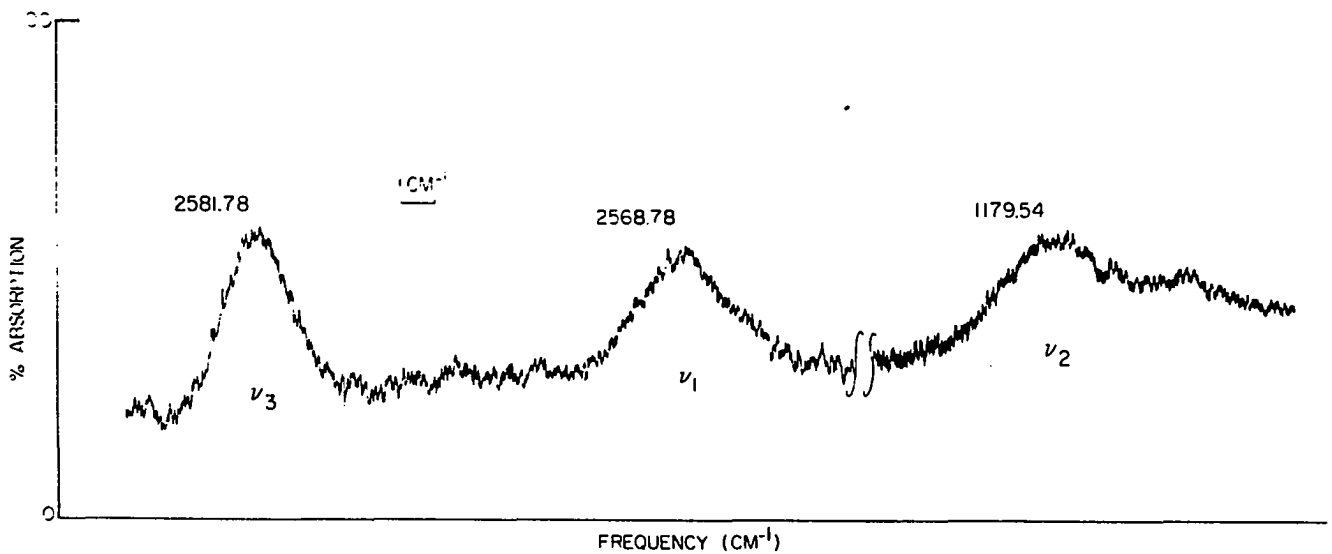

Fig. II.E.1. The infrared spectrum of H_2S in solid argon at 8°K

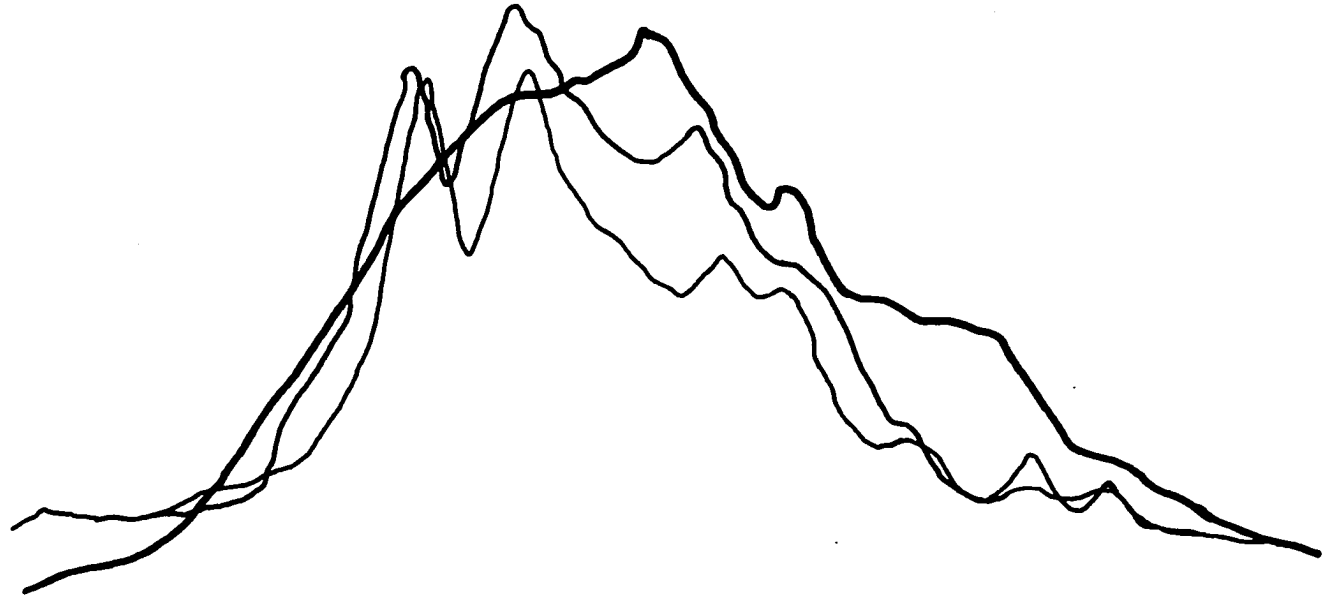

Fig. II.E.2. Diffusion experiment for D_2S in krypton

III. MATRIX SPECTRA OF HCN IN ARGON: AN EXAMINATION OF THE ASSUMPTIONS OF THE MATRIX ISOLATION TECHNIQUE

A. Experimental

1. Technique

HCN was prepared in a vacuum system by condensing H_2O onto an equimolar mixture of reagent grade KCN and P_2O_5 at a liquid nitrogen temperatures. After the mixture was slowly warmed to room temperature, the HCN was distilled and repeatedly condensed on P_2O_5 to remove traces of water.

Several samples were analyzed by mass spectrometry and found to contain peaks attributable to HCN only; however, if the KCN, P_2O_5, and H_2O mixture was not allowed to warm slowly a peak at mass = 52 appeared. This peak was attributed to $(CN)_2$. No $(CN)_2$ was present in the samples used for matrix isolation.

The experimental apparatus was identical to that used in the H_2S studies with the exception that an all glass vacuum system was used in place of a copper vacuum system.

All sample concentrations were 1/700 or 1/350 mole ratio HCN/Ar. The deposition rate was 0.04 millimoles/min. and the deposition temperature was approximately 20°K. All spectra were recorded at 10°K.

The spectra were calibrated using gas phase HCN (34), DCN (9), and H_2O (16).

2. Spectra

a. ν_3 region Fig. III.A.1 contains spectra of ν_3 for $H^{13}C^{14}N$ and $H^{12}C^{15}N$. The spectrum for the N^{15} isotope was recorded at a slower

chart speed to show the slight asymmetric character of the ν_3 band. Fig. III.A.2 shows spectra for ν_3 of $D^{12}C^{14}N$ and $D^{13}C^{14}N$. The spectra for other isotopes are identical to those in the above figures. Spectral widths, band centers and frequency dispersions are noted on the figures.

b. ν_2 region Fig. III.A.3 shows the spectra of ν_2 for $D^{12}C^{14}N$ and $D^{13}C^{14}N$. The spectra for the other isotopes in the ν_2 region are similar to those shown in Fig. III.A.3.

c. ν_1 region Fig. III.A.4 shows four concentration experiments of the ν_1 region of $H^{12}C^{14}N$. No other features were observed other than those shown in the figure. The large increase in intensity of the large band at 2110 cm^{-1} with increasing concentration of HCN strongly suggests that it arose from polymeric species. This band coincides with a very strong absorption of solid HCN (20). The diffusion experiment in Fig. III.A.5 supports this view. Both the 2110 and 2095 cm^{-1} absorptions increase in intensity while the 2115 cm^{-1} absorption irreversibly decreases in intensity after diffusion. On the other hand, the ν_1 band of DCN was unambiguously observed. Fig. III.A.6 shows the spectra for ν_1 of $D^{12}C^{15}N$. The spectra for the $D^{12}C^{14}N$ and $D^{13}C^{14}N$ isotopes are similar. The ν_1 bands for the deuterium isotopes are not complicated by polymer bands in this region and the intensity of ν_1 bands for DCN is approximately 20 times stronger than ν_1 of HCN (21). The isotopic shifts for DCN to HCN implies ν_1 of HCN should absorb at 2095 cm^{-1} which is buried in a polymer band. Since solid HCN exhibits intense polymer bands in this region, no assignment of ν_1 was made for HCN.

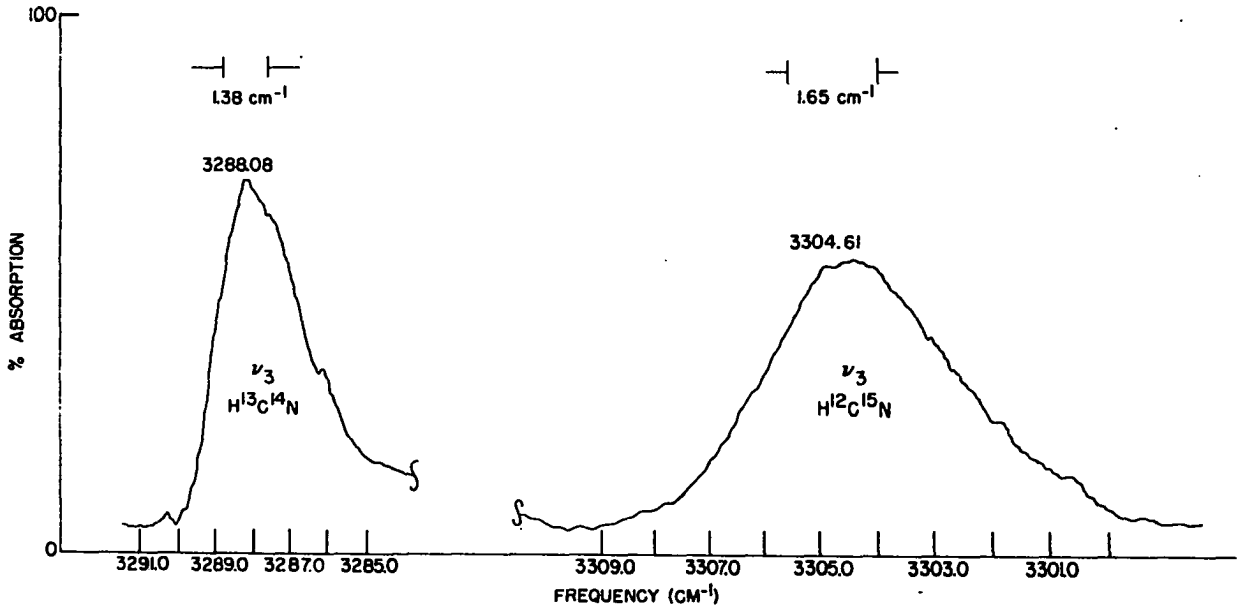

Fig. III.A.1. Spectra of ν_3 for $H^{13}C^{14}N$ and $H^{12}C^{15}N$

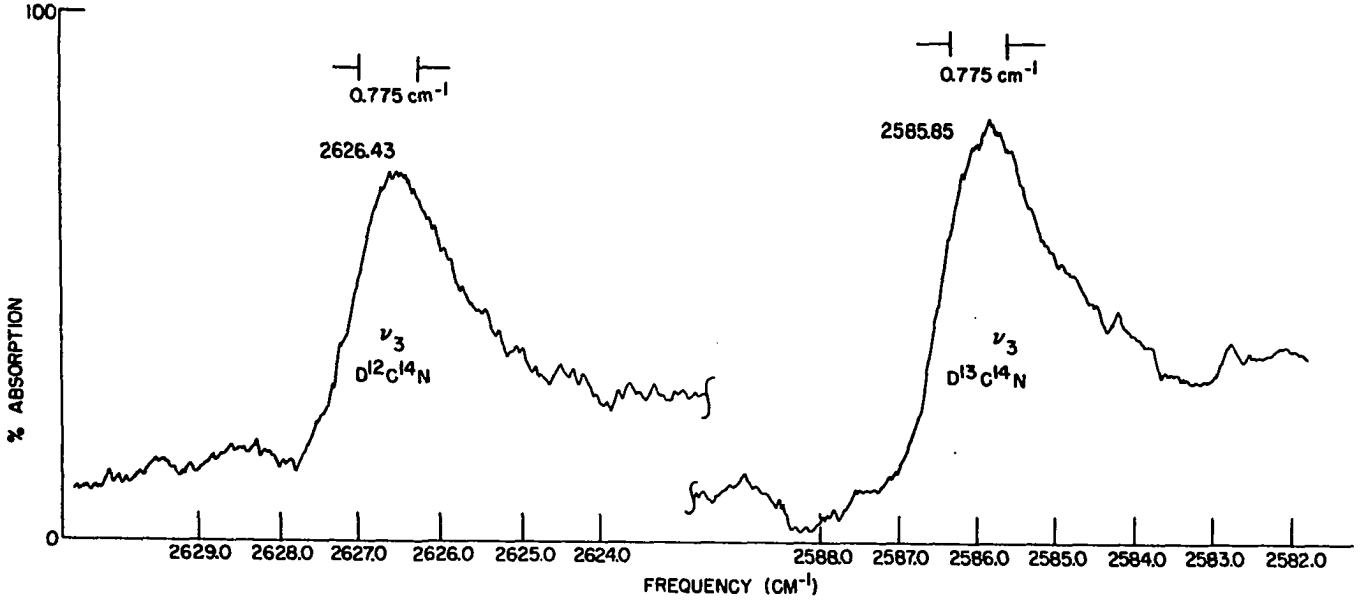

Fig. III.A.2. Spectra for ν_3 of $D^{12}C^{14}N$ and $D^{13}C^{14}N$

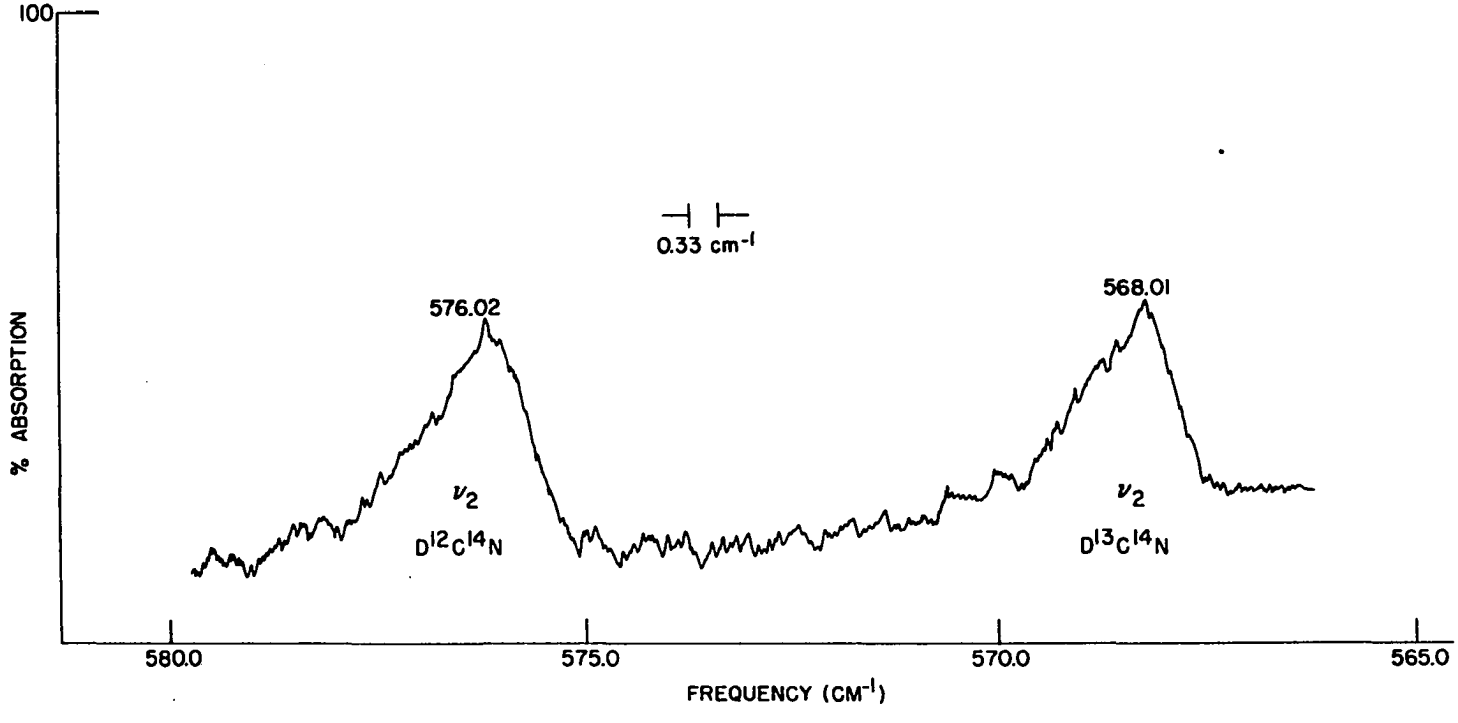

Fig. III.A.3. Spectra of ν_2 for $D^{12}C^{14}N$ and $D^{13}C^{14}N$

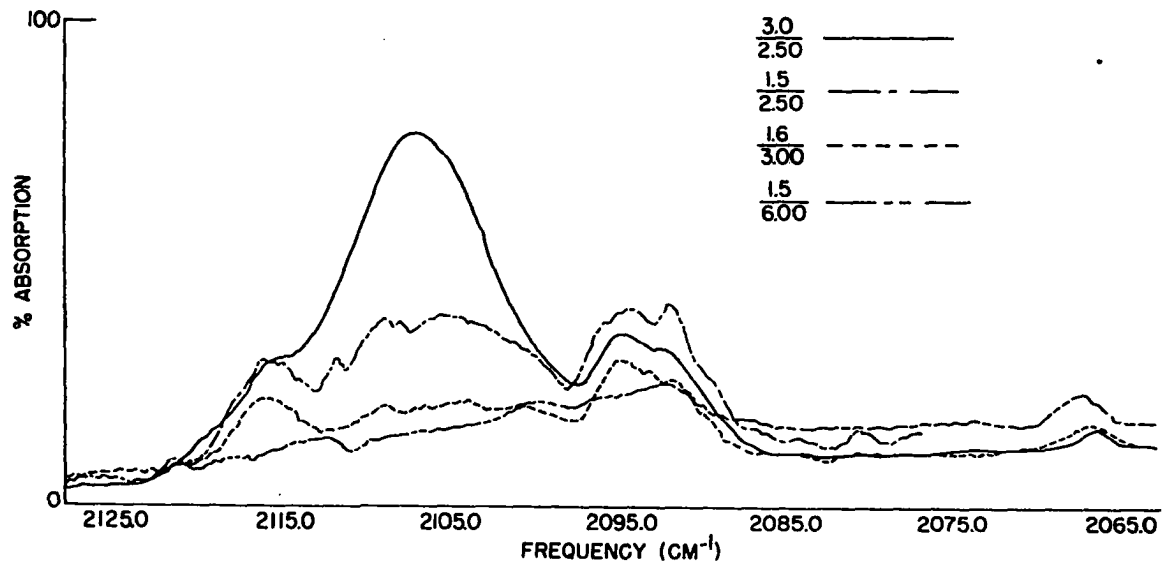

Fig. III.A.4. Concentration dependence of $H^{12}C^{14}N$ in the ν_1 region

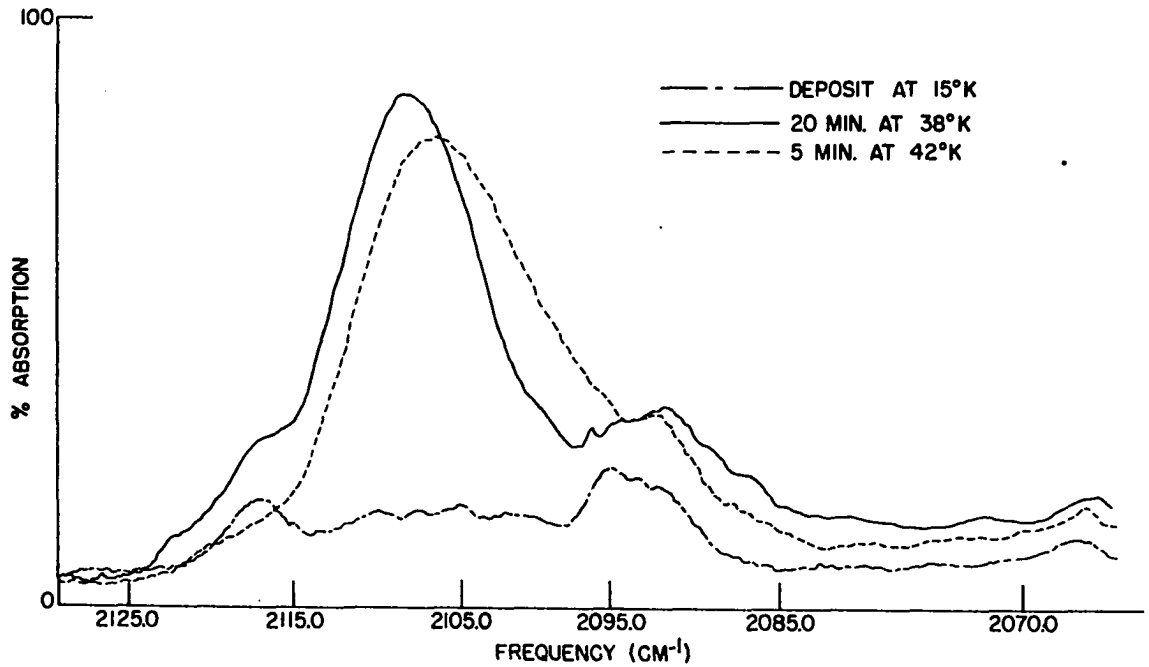

Fig. III.A.5. Diffusion experiment for $H^{12}C^{14}N$ in the ν_1 region

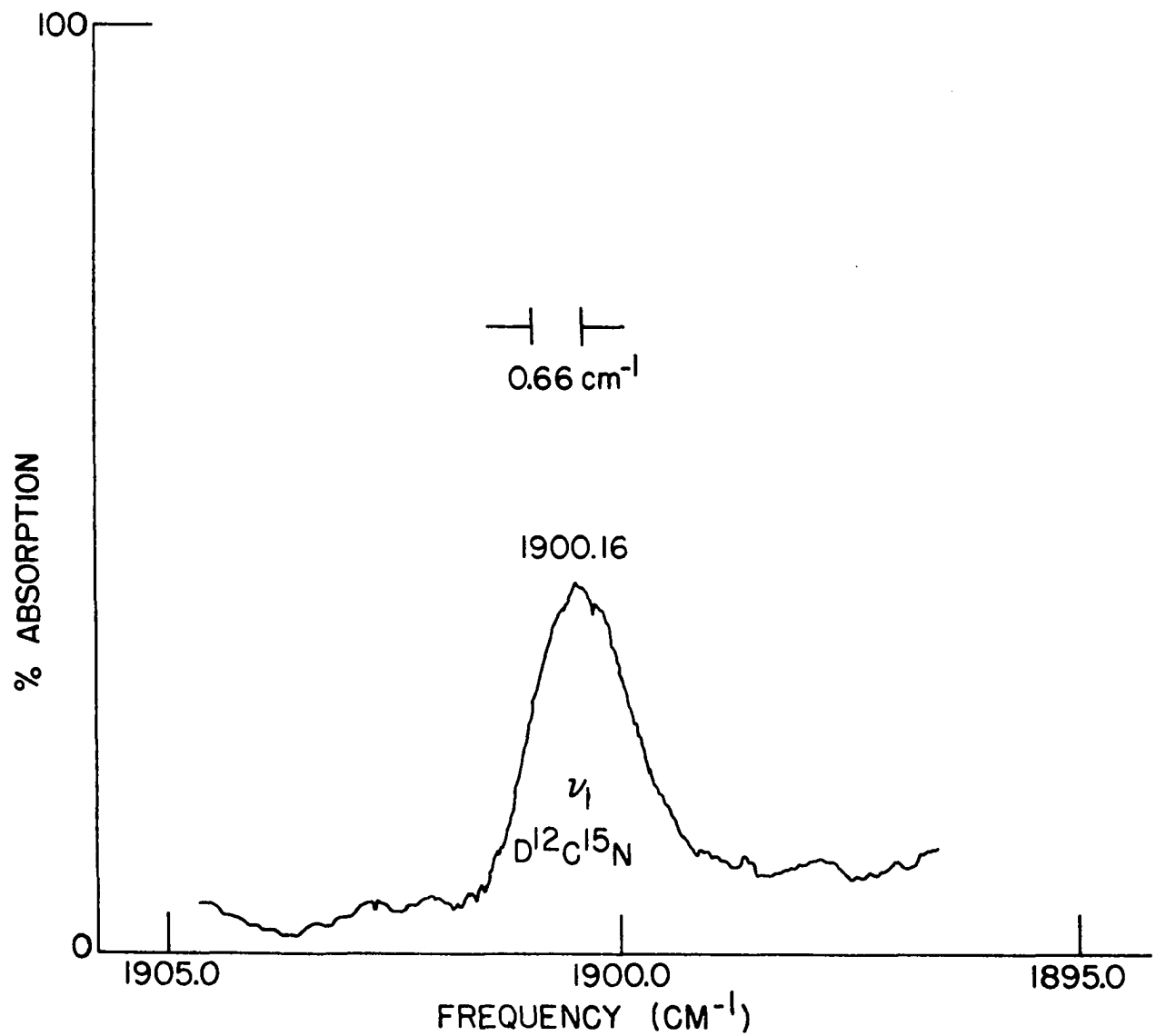

Fig. III.A.6. Spectrum for ν_1 of $D^{12}C^{15}N$

3. Results

Table III.A.1 contains the calibrated matrix frequencies, the average deviations and the number of calibrations measured for each band. Table III.A.2 contains the gas phase band centers and harmonic frequencies tabulated by Nakagawa and Morino (28).

In Table III.A.3 the matrix shifts $\delta \nu_i = \nu_i^m - \nu_i^g$, are reported. The shift for ν_1 is very small, ν_2 is shifted to higher frequencies and ν_3 is shifted to lower frequencies.

A discrepancy between isotopic shifts in the matrix and the gas phase was previously noted for H_2S and D_2S. This same discrepancy is noted for HCN in Table III.A.4. Define $\Delta_i^g = \nu_i^g - \nu_i^{g'}$ as the isotopic shift in the gas; then $\Delta_i' = \Delta_i^m - \Delta_i^g$ is the difference between the isotopic shifts for the gas and matrix frequencies. Table III.A.4 shows that Δ_i' is small for small isotopic mass changes (C^{12} to C^{13}, N^{14} to N^{15}) while Δ_i' is large for large isotopic mass changes (H to D).

The significance of the matrix isotopic descrepancies is illustrated by an example. Several groups (8,24) have studied the high resolution matrix isolation infrared spectra of symmetric bent triatomic molecules. They have measured band centers within $\pm$ 0.05 cm^{-1} in order to accurately determine the bond angle which is calculated from the expression

$$(\omega_3/\omega_3')^2 = [\mu_X + \mu_Y(1 - \cos\alpha)]/[\mu_X + \mu_Y'(1 - \cos\alpha)] \qquad \text{(III.A.1)}$$

where ω_3, ω_3' are the isotopic harmonic asymmetric stretching frequencies, and α is the bond angle. An assumption made because of the

Table III.A.1. Calibrated matrix frequencies of HCN in argon

	ν_1	A.D.[a]	T[b]	ν_2	A.D.[a]	T[b]	ν_3	A.D.[a]	T[b]
$H^{12}C^{14}N$				720.96	.05	10	3305.66	.07	4
$H^{13}C^{14}N$				714.94	.03	8	3288.08	.13	6
$H^{12}C^{15}N$				719.74	.04	4	3304.61	.10	4
$D^{12}C^{14}N$	1925.17	0.03	4	576.02	.05	4	2626.43	.05	4
$D^{13}C^{14}N$	1911.91	0.01	3	568.01	.06	4	2585.85	.03	6
$D^{12}C^{15}N$	1900.16	0.01	3	574.44	.02	6	2616.99	.02	4

[a]A.D. = average deviation.

[b]T = number of trials.

Table III.A.2. HCN gas phase frequencies

	ν_1	ν_2	ν_3	ω_1	ω_2	ω_3
$H^{12}C^{14}N$	2096.85	712.35	3311.45	2128.67	727.10	3441.16
$H^{13}C^{14}N$	2063.05	706.34	3293.46	2094.16	720.71	3422.04
$H^{12}C^{15}N$	2064.35	711.41	3310.13	2095.12	726.01	3439.85
$D^{12}C^{14}N$	1925.24	569.30	2630.34	1952.12	579.85	2703.34
$D^{13}C^{14}N$	1911.81	561.60	2590.05	1938.52	571.82	2661.58
$D^{12}C^{15}N$	1900.12	568.06	2621.22	1925.83	578.49	2694.30

Table III.A.3. Observed matrix shifts

	$\delta\nu_1$	$\delta\nu_2$	$\delta\nu_3$
$H^{12}C^{14}N$		8.61	-5.84
$H^{13}C^{14}N$		8.60	-5.38
$H^{12}C^{15}N$		8.33	-5.52
$D^{12}C^{14}N$	-0.07	6.72	-3.91
$D^{13}C^{14}N$	0.10	6.41	-4.20
$D^{12}C^{15}N$	0.04	6.38	-4.23

Table III.A.4. Gas phase and matrix isotopic frequency shifts

	Δ_1^{m}[a]	Δ_1^{g}[b]	Δ_1'[c]	Δ_2^{m}	Δ_2^{g}	Δ_2'[d]	Δ_3^{m}	Δ_3^{g}	Δ_3'[e]
$H^{12}C^{14}N$									
$H^{13}C^{14}N$				6.02	6.00	0.02	17.53	17.99	-0.46
$H^{12}C^{14}N$									
$H^{12}C^{15}N$				1.22	0.94	-0.28	1.00	1.32	-0.32
$D^{12}C^{14}N$									
$D^{13}C^{14}N$	13.26	13.43	-0.17	8.01	7.70	0.31	40.58	40.29	0.29
$D^{12}C^{14}N$									
$D^{12}C^{15}N$	25.01	25.12	-0.11	1.58	1.24	0.24	9.44	9.12	0.32
$H^{12}C^{14}N$									
$D^{12}C^{14}N$				144.94	143.05	1.89	679.18	681.11	-1.93
$D^{13}C^{14}N$									
$D^{13}C^{14}N$				146.93	144.74	2.19	702.23	703.41	-1.18
$H^{12}C^{15}N$									
$D^{12}C^{15}N$				145.30	143.35	1.95	687.62	688.91	-1.29

[a] $\Delta_i^{m} = \nu_i^{m} - \nu_i^{m'}$.

[b] $\Delta_i^{g} = \nu_i^{g} - \nu_i^{g'}$.

[c] $\Delta_i' = \Delta_i^{m} - \Delta_i^{g'}$.

[d] Estimated average deviation ± 0.20.

[e] Estimated average deviation ± 0.20.

use of matrix data instead of gas phase data in Eq. III.A.1 is that the frequencies shift nearly the same amount and thus have little effect on the frequency ratio. The Δ_i in Table II.E.4 for H_2S and D_2S show that this assumption is poor for H to D isotopic substitution. Furthermore, since the bond angle is sensitive function of vibrational frequencies then a poor value for the bond angle will be calculated regardless of the accuracy of bond center measurements, unless $\Delta'_i \approx 0$ or within experimental uncertainty.

The isotopic discrepancies can arise from several effects which are discussed after the important matter of anharmonicities is investigated in the following section.

B. Determination of Anharmonicities

1. Matrix anharmonicities

Several attempts are made to determine anharmonicities in the matrix. The first is a general method while the second involves the Redlich-Teller Product Rule. Reasons are given why the methods fail to yield matrix anharmonicities.

The general expressions relating the observed and harmonic fundamental vibrational frequencies for a particular isotope of HCN are

$$\begin{aligned} \nu_1 &= \omega_1 + 2X_{11} + X_{12}/2 + X_{13}/2 \\ \nu_2 &= \omega_2 + 3X_{22} + X_{12} + X_{23} + X_{LL} \\ \nu_3 &= \omega_3 + 2X_{33} + X_{13}/2 + X_{23}/2 \end{aligned} \qquad \text{(III.B.1)}$$

where ν_i and ω_i are the observed and harmonic frequencies, X_{ii} and X_{ij} are the corrections for the anharmonicities of the i and j vibrations, and X_{LL} is the anharmonicity contribution which arises from the degeneracy of the ν_2 fundamental. For each isotope of HCN one obtains a similar expression as illustrated below for three isotopic species of ν_1':

$$\nu_1 = \omega_1 + 2X_{11} + X_{12}/2 + X_{13}/2$$

$$\nu_1' = \omega_1' + 2X_{11}' + X_{12}'/2 + X_{13}'/2 \qquad \text{(III.B.2)}$$

$$\nu_1'' = \omega_1'' + 2X_{11}'' + X_{12}''/2 + X_{13}''/2$$

By use of Dennison's Rule,

$$X_{ij}'/X_{ij} = \omega_i'\omega_j'/\omega_i\omega_j \approx \nu_i'\nu_j'/\nu_i\nu_j \qquad \text{(III.B.3)}$$

the X_{ij} can be related to X_{ij}' and X_{ij}''. In addition, if one assumes the X_{LL} are the same in the gas phase and in the matrix, the nine equations for the various ν_i's can be solved in terms of nine unknowns--the three ω_i's and six X_{ij}'s. An attempt to use this procecure for $D^{12}C^{14}N$, $D^{13}C^{14}N$, $D^{12}C^{15}N$ failed for two reasons: first the Eqs. III.B.2 are nearly co-linear, and second, some of the C^{12}-C^{13}, N^{14}-N^{15} isotopic shifts are so small that the approximations made are not valid.

Thus another approach had to be tried to determine the anharmonicities. The total anharmonicity correction for ν_2, denoted α_2, can be written:

$$\nu_2 = \omega_2(1 - \alpha_2) \qquad \text{(III.B.4)}$$

Using the Redlich-Teller Product Rule,

$$\omega_2'/\omega_2 = |G'| / |G| \qquad \text{(III.B.5)}$$

where $|G|$ is the determinant of $\tilde{G}$; and the Dennison Rule:

$$\alpha_2'/\alpha_2 = \omega_2'/\omega_2 \qquad \text{(III.B.6)}$$

α_2 can be determined. This method also failed because the empirical Dennison Rule is not valid for HCN. The reason for the failure can be seen by rewriting α_2 in terms of the X_{ij} and ω_2:

$$\alpha_2'/\alpha_2 = (\omega_2/\omega_2')[3X_{22}' + X_{12}' + X_{23}' + X_{LL}']/$$

$$[3X_{22} + X_{12} + X_{23} + X_{LL}]$$

Using Dennison's Rule,

$$\alpha_2'/\alpha_2 = (\omega_2/\omega_2')[3(\omega_2'/\omega_2)^2 X_{22} + (\omega_1'\omega_2'/\omega_1\omega_2)X_{12} +$$

$$X_{LL}(\omega_2'/\omega_2)^2]/(3X_{22} + X_{12} + X_{23} + X_{LL}) \qquad \text{(III.B.7)}$$

The equality $\alpha_2'/\alpha_2 = \omega_2'/\omega_2$ requires that $\omega_1'/\omega_1 \approx \omega_2'/\omega_2 \approx \omega_3'/\omega_3$ a condition which is not met in this case. This is illustrated in Table III.B.3 where it appears that the condition is met for C^{12} to C^{13} and N^{14} to N^{15} isotopic pairs. However, the method also fails in these cases because the isotopic frequency shifts are so small that the error propagation makes the α_i's very inaccurate.

Several studies have shown that anharmonicities can be transferred from the gas phase to the matrix (8,24). The various α's are shown in

Table III.B.1 and were calculated on this basis. The harmonic frequencies in the matrix using the gas phase α_i (28) are shown in Table III.B.2.

2. The effect of changes in anharmonicity

Maki (23) studied the infrared spectrum of $C^{12}O^{16}$ and concluded that the anharmonic constant in the solid was the same as the anharmonic constant in the gas. It would be desirable to use a similar procedure for HCN, assuming that the matrix harmonic frequencies were equal to those for the gas phase and using the observed matrix frequencies to find the various X_{ij}'s. These could be compared to the gas phase X_{ij}'s to determine if "reasonable" changes account for the observed matrix shifts.

In the application of this method for HCN and DCN other assumptions were necessary; first, ν_1 for HCN in the matrix was set equal to ν_1 in the gas phase, and second, X_{11}, X_{12}, X_{13} for both isotopes in the matrix were set equal to their gas phase values. This method worked poorly because of the uncertainty of several gas phase X_{ij} (28).

An alternate procedure was used to compare gas and matrix anharmonicities. The Redlich-Teller Product Rule for ν_1 and ν_3 is

$$\omega_1'\omega_3'/\omega_1\omega_3 = \pi = \nu_1'\nu_3'(1 - \alpha_1)(1 - \alpha_3)/$$

$$(1 - \alpha_1')(1 - \alpha_3')\nu_1\nu_3 \qquad \text{(III.B.8)}$$

Rearranging the equation gives

$$(1 - \alpha_3)/(1 - \alpha_3') = \pi = \nu_1\nu_3(1 - \alpha_1')/\nu_1'\nu_3'(1 - \alpha_1) \qquad \text{(III.B.9)}$$

Eq. III.B.9 is used to find the ratio of the anharmonicities in either

Table III.B.1. Gas phase anharmonicities[a]

	$H^{12}C^{14}N$	$H^{13}C^{14}N$	$H^{12}C^{15}N$	$D^{12}C^{14}N$	$D^{13}C^{14}N$	$D^{12}C^{15}N$
α_1	0.014948	0.014856	0.014687	0.013770	0.013779	0.013350
α_2	0.020286	0.019939	0.020110	0.018194	0.0178273	0.018030
α_3	0.037694	0.037574	0.037711	0.02700	0.026875	0.027121

[a]Source: (28).

Table III.B.2. Harmonic matrix frequencies

	ω_1	ω_2	ω_3
$H^{12}C^{14}N$		735.89	3435.09
$H^{13}C^{14}N$		729.48	3416.33
$H^{12}C^{15}N$		734.51	3434.11
$D^{12}C^{14}N$	1952.05	586.70	2699.32
$D^{13}C^{14}N$	1938.62	578.35	2657.26
$D^{12}C^{15}N$	1925.87	584.99	2689.95

Table III.B.3. Ratio of isotopic gas phase frequencies

	ω_1'/ω_1	ω_2'/ω_2	ω_3'/ω_3
$H^{12}C^{14}N$ / $H^{13}C^{14}N$	0.98379	0.99121	0.99440
$H^{12}C^{14}N$ / $H^{12}C^{15}N$	0.98424	0.99850	0.99962
$H^{12}C^{14}N$ / $D^{12}C^{14}N$	0.91706	0.79748	0.78559
$D^{12}C^{14}N$ / $D^{13}C^{14}N$	0.99303	0.98615	0.98455
$D^{12}C^{14}N$ / $D^{12}C^{15}N$	0.98617	0.99766	0.99666

Table III.B.4. Ratios for the gas phase and matrix anharmonicities

	$H^{12}C^{14}N$ / $D^{12}C^{14}N$	$H^{13}C^{14}N$ / $D^{13}C^{14}N$	$H^{12}C^{15}N$ / $D^{12}C^{15}N$	$H^{12}C^{14}N$ / $H^{13}C^{14}N$	$H^{12}C^{14}N$ / $H^{12}C^{15}N$	$D^{12}C^{14}N$ / $D^{13}C^{14}N$	$D^{12}C^{14}N$ / $D^{12}C^{15}N$
$[(1 - \alpha_3)/(1 - \alpha_3')]_m$	0.9888	0.9890	0.9891	0.9998	0.9999	0.9999	1.0002
$[(1 - \alpha_3)/(1 - \alpha_3')]_g$	0.9890	0.9890	0.9891	0.9999	1.0000	0.9987	1.0001
$[(1 - \alpha_2)/(1 - \alpha_2')]_m$	0.9982	0.9990	0.9981	0.9996	1.0002	1.0001	1.0004
$[(1 - \alpha_2)/(1 - \alpha_2')]_g$	0.9979	0.9979	0.9979	0.9997	0.9998	0.9997	0.9998

the matrix or gas phase. In Eq. III.B.9 the assumption is made that the anharmonicity of the CN stretch α_1, is the same in the gas phase and matrix, the validity of this depends on the near coincidence of the gas and matrix frequencies.

Similarly the product rule for the bending mode ν_2 gives

$$(1 - \alpha_2)/(1 - \alpha_2') = \omega_2' \nu_2/\omega_2 \nu_2' = \pi \nu_2/\nu_2' \quad \text{(III.B.10)}$$

Table III.B.4 shows the ratios for all possible isotopes. All of the ratios are in good agreement. Thus, to the extent that the ratios are sensitive measures of anharmonicity changes, the differences between gas phase and matrix anharmonicities are undetectable by our measurements.

C. Force Constants: Linear XYZ Model

To calculate the force constants in an argon matrix from the harmonic frequencies given in Table III.B.2, two assumptions are made: first, that no geometry changes occur in the matrix environment and second, that the linear XYZ model used to calculate the force constants in the gas phase is appropriate for calculating the force constants in the matrix. Under these assumptions the force constants were calculated using the gas phase geometries given in Table III.C.1 and the following expressions:

$$\lambda_1 + \lambda_3 = f_{CN}(\mu_C + \mu_N) - f_{CH}(\mu_H + \mu_C) \quad \text{(III.C.1)}$$

$$\lambda_1 \lambda_3 = [\, f_{CN}(\mu_C + \mu_N) - f_{rr}\mu_C] \times [\, f_{CH}(\mu_H + \mu_C) - f_{rr}\mu_C] \quad \text{(III.C.2)}$$

Table III.C.1. Gas Phase Geometry of HCN[a]

	r_{CH}	r_{CN}	r_{CN}/r_{CH}
Hydrogen	1.0674	1.1557	1.0827
Deuterium	1.0658	1.1555	1.08416

[a]Source: (7,38).

Table III.C.2. Matrix and gas stretching force constants for linear XYZ model

	Matrix[a]	Gas[a]
f_{CH}	6.165	6.209
f_{CN}	18.869	18.712
f_{rr}	-0.219	-0.228

[a]All force constants calculated from deuterium isotopes.

Table III.C.3. Matrix and gas bending force constants for linear XYZ model

	Matrix[a]	Gas
$H^{12}C^{14}N$	0.2669	0.2606
$H^{13}C^{14}N$	0.2670	0.2607
$H^{12}C^{15}N$	0.2667	0.2606
$H^{12}C^{14}N$	0.2663	0.2601
$D^{13}C^{14}N$	0.2660	0.2600
$D^{12}C^{15}N$	0.2659	0.2601

[a]Calculated under the assumption gas phase geometry is transferable to the matrix.

$$\lambda_2 = f_\theta \left[\mu_H/r_{CH}^2 + \mu_N/r_{CH}^2 + \mu_C(1/r_{CH} + 1/r_{CN})^2\right] \qquad \text{(III.C.3)}$$

Here μ_C, μ_N, and μ_H are the reciprocal masses of the carbon, nitrogen and hydrogen atoms, r_{CH} and r_{CN} are the equilibrium bond lengths for the CH and CN bonds and f_{CH}, f_{CN}, f_{rr} are the force constants for the CH and CN bonds and the stretch-stretch interaction constant respectively. The force constants could only be completely determined for the deuterium isotopic frequencies since ν_1 was not observed for the hydrogen isotopes. The bending force constant f_θ, however was calculated for each isotope. The gas phase and matrix force constants are shown in Tables III.C.2 and III.C.3. Note the decrease in f_{CH} and increase in f_{CN} and f_θ compared to the gas phase values. These small discrepancies are outside the limits of experimental error. They can arise from two effects: changes in geometry and an inappropriate vibrational model. The following sections explore these possibilities and their influence on matrix shifts.

D. Effect of the Matrix on Molecular Geometry

In this section the ratio of the bond lengths r_{CH}/r_{CN} are found and compared to r_{CH}/r_{CN} in the gas phase. The ratios show that the geometry of HCN in a matrix environment cannot be found using a linear XYZ vibrational model. Also, a model for HCN in a spherical cavity of argon atoms is developed which predicts that the geometry of HCN in a matrix is essentially identical to that in the gas phase.

When HCN is isolated in an argon matrix the following assumptions

pertinent to geometry changes caused by the solvent are made: first, the molecule remains linear, consequently, any geometry changes are a result of changes in the CH or CN bond lengths; and second, the potential energy surfaces for all of the isotopes of HCN in argon are identical.

The eigenvalue for the bending mode of HCN is given by Eq. III.C.3. For the two isotopes XYZ and X'YZ the differences in the eigenvalues of ν_2,

$$\lambda_2 - \lambda_2' = f_\theta \, (\mu_X - \mu_X')/r_{XY} \qquad \text{(III.D.1)}$$

can be rearranged to give an expression for r_{YZ}/r_{XY} which is independent of f_θ. For the isotopic species $H^{12}C^{14}N$, $D^{12}C^{14}N$, and $H^{12}C^{15}N$, this ratio is

$$r_{CN}/r_{CH} = [(\lambda_2(H^{12}C^{14}N) - \lambda_2(D^{12}C^{14}N)(\mu^{14} - \mu^{15})/$$
$$(\lambda_2(H^{12}C^{14}N) - \lambda_2(H^{12}C^{15}N))(\mu_H - \mu_D)]^{1/2} \qquad \text{(III.D.2)}$$

A comparison of the ratio calculated from argon matrix data to the ratio found in the gas phase can be interpreted as a measure of geometry change caused by the solvent. Since the CN bond is very strong and the CN stretching has a small solvent shift one expects r_{CN} to be relatively unaffected by the solvent. On the other hand, the larger solvent shifts shown by the CH stretching frequency leads one to presume that changes in the bond length ratios in the matrix to be largely caused by changes in r_{CH}.

A number of ratios calculated from observed and harmonic matrix and gas frequencies are shown in Table III.D.1. The averages for ratios obtained from the harmonic frequencies shows a much longer r_{CH} in the matrix than in the gas. One finds the various $(r_{CH}/r_{CN})\omega_2$ in the gas phase agree to within $\pm$ 0.005 to the ratio $r_{CH}/r_{CN} = 1.080$ found from microwave data as shown in

Table III.C.1. Such agreement is not found for the matrix ratios. The experimental uncertainties for the harmonic matrix ratio shown in the third column of Table III.D.1 indicate that the disagreement in the ratios is outside the range of experimental error. Since the gas phase ratios agree, and the ratios in the matrix are not only much different but are discordant one must consider that the source of the discrepancy is either (A) a real change in the geometry or (B) due to the inapplicability of the linear XYZ vibrational model in the matrix.

An independent estimate of geometry changes to be expected when HCN is placed in an argon matrix can be made. Presume that each HCN molecule is trapped in a spherical cavity of argon atoms which interacts with the hydrogen and nitrogen ends of the HCN molecule. These interactions are described by a Lennard-Jones intermolecular potential function averaged over the spherical cavity. The total potential then is the sum of the spherically averaged potentials plus the harmonic oscillator potentials for the CH and CN bonds. The equilibrium geometry of HCN for a particular cavity size can be found by minimization of the total potential with respect to the positions of the hydrogen, carbon and nitrogen atoms in the cavity.

The model is developed in Appendix C. The results of this spherical cell model gives for the total potential energy of the system,

$$\chi(a,b,c,R) = \sum_{i=1} n_i[\psi(a,R_i) + \xi(c,R_i)] + \phi_{CH} + \phi_{CN} \qquad \text{(III.D.3)}$$

where n_i is the number of argon atoms at the surface of a spherical shell of radius R_i and is calculated from the following equation:

$$n_i = 12.0(R_i/1.91)^2$$

where the 12.0 refers to the number of nearest neighbors and 1.91 is the Van der Waals radius of an argon atom; $\psi(a,R_i)$ and $\xi(c,R_i)$ are the spherically averaged Lennard-Jones interactions for the Ar-H and Ar-N ends of the HCN molecule. (See Eq. VI.C.9) ϕ_{CH} and ϕ_{CN} are the harmonic potential functions for the CH and CN bonds; (See Eqs. VI.C13 and VI.C.14) a, b, and c are the distances for the hydrogen, carbon and nitrogen atoms from the origin which is the center of the cavity.

Minimization of $\chi(a,b,c,R)$ for a particular cavity size R allows a determination of the equilibrium positions of hydrogen, carbon and nitrogen atoms in the cavity, hence the equilibrium geometry of HCN as well as the position of the molecule in the cavity.

The parameters used in the minimization process for the Lennard-Jones potential are given in Table III. D.2 where ϵ and σ correspond to the depth of the well and the internuclear distance of closest approach of two molecules or atoms as shown in Fig. III. D.1. The usual arithmetic and geometric mean is used to obtain the mixed ϵ's and σ's as illustrated in Table III.D.2.

The inclusion of spherical shells of argon atoms, other than the first shell, had a negligible effect on the other minimum parameters, therefore, only the first shell was retained. Fig. III.D.2 is a plot of the lowest value of χ found for each cavity size. The function reaches its lowest value at R = 3.92 A. If the inter and intra-molecular equilibrium distances are added for Ar-H, Ar-N, CH and CN, a value of 4.17 A is obtained, whereas adding contact distance, σ_{ArH}, σ_{ArH}, r_{CN} and r_{CH} gives

3.83 A. This leads to the conclusion that the H and N ends of the HCN molecule are close or at Van der Waals contact distances.

Fig. III.D.3 is a plot of the positions of the H, C, and N atoms as a function of cavity size. The center of the cavity is taken as the origin with the H atom negative and the N atom positive. The plot consists of three very similar curves. The only difference is they are shifted by an amount which corresponds to the r_{CN} and r_{CH} equilibrium bond lengths. The plot reveals that the molecule adjusts itself essentially like a rigid body in the cavity in order to minimize the total potential. There is very little change in r_{CH} or r_{CN} bond lengths until the cavity radius is less than 3.8 A; then the repulsive potential compresses the molecule. At values of R more than 3.8 A the molecule moves over to the Ar-H side of the cavity because of the stronger Ar-H Lennard-Jones parameters.

Fig. III.D.4 shows a plot of the r_{CN} and r_{CH} equilibrium distances as a function of cavity size. Below R = 4.0 A the cavity decreases the bond lengths while above 4.0 A the cavity increases the bond lengths slightly. At the equilibrium cavity size R = 3.92 A, the r_{CH} = 1.065 A, r_{CN} = 1.155 A where in the gas phase r_{CH} = 1.067 A and r_{CN} = 1.155 A. Thus, the effect of the matrix on the geometry of the HCN molecule is very small and undetectable by present matrix spectroscopic methods.

The discrepancy observed in the bond length ratios of HCN in argon cannot be due to a real geometry change. Hence, other vibrational models for HCN in an argon matrix are explored in the next section.

Table III.D.1. Ratios of gas phase and matrix bond lengths

	Matrix $(r_{CN}/r_{CH})\omega_2$	Gas $(r_{CN}/r_{CH})\omega_2$
$H^{12}C^{14}N$ - $D^{12}C^{14}N$ $H^{12}C^{14}N$ - $H^{12}C^{15}N$	0.9649 ± 0.03	1.079
$H^{12}C^{14}N$ - $D^{12}C^{14}N$ $D^{12}C^{14}N$ - $D^{12}C^{15}N$	0.9711 ± 0.03	1.082
$H^{12}C^{14}N$ - $D^{12}C^{14}N$ $H^{12}C^{14}N$ - $H^{13}C^{14}N$	1.092 ± 0.02	1.081
$H^{12}C^{14}N$ - $D^{12}C^{14}N$ $D^{12}C^{14}N$ - $D^{13}C^{14}N$	1.053 ± 0.02	1.081
$H^{12}C^{14}N$ - $H^{13}C^{14}N$ $H^{12}C^{14}N$ - $H^{12}C^{15}N$	0.8486 ± 0.05	1.077
$D^{12}C^{k4}N$ - $D^{13}C^{14}N$ $D^{12}C^{14}N$ - $D^{12}C^{15}N$	0.8888 ± 0.05	1.082
Average	0.9700 ± 0.04	1.080

Table III.D.2. Lennard-Jones Parameters for the spherical model

	Ar	N_2	CH_4	Ar-H	Ar-N
ϵ	116	79.8	144	129.2[a]	96.2[a]
σ	3.465	3.749	3.796	2.538[b]	2.907[b]

[a] $\epsilon_{Ar-H} = (\epsilon_{Ar}\epsilon_{CH_4})^{1/2}$

$\epsilon_{Ar-N} = (\epsilon_{Ar}\epsilon_{N_2})^{1/2}$

[b] $\sigma_{Ar-H} = (\sigma_{Ar} + \sigma_{CH_4})/2 - r_{CH}(CH_4)$

$\sigma_{Ar-N} = (\sigma_{Ar} + \sigma_{CH_4})/2$ - covalent radius of N in N_2

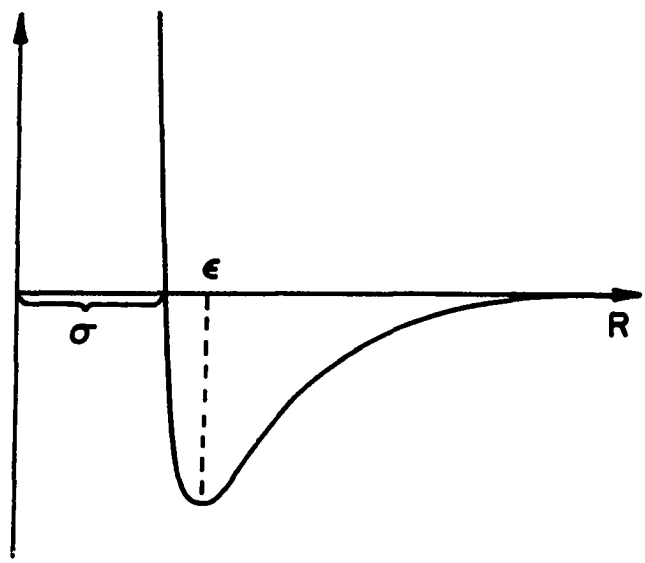

Fig. III.D.1. Shape and parameters for the Lennard-Jones potential

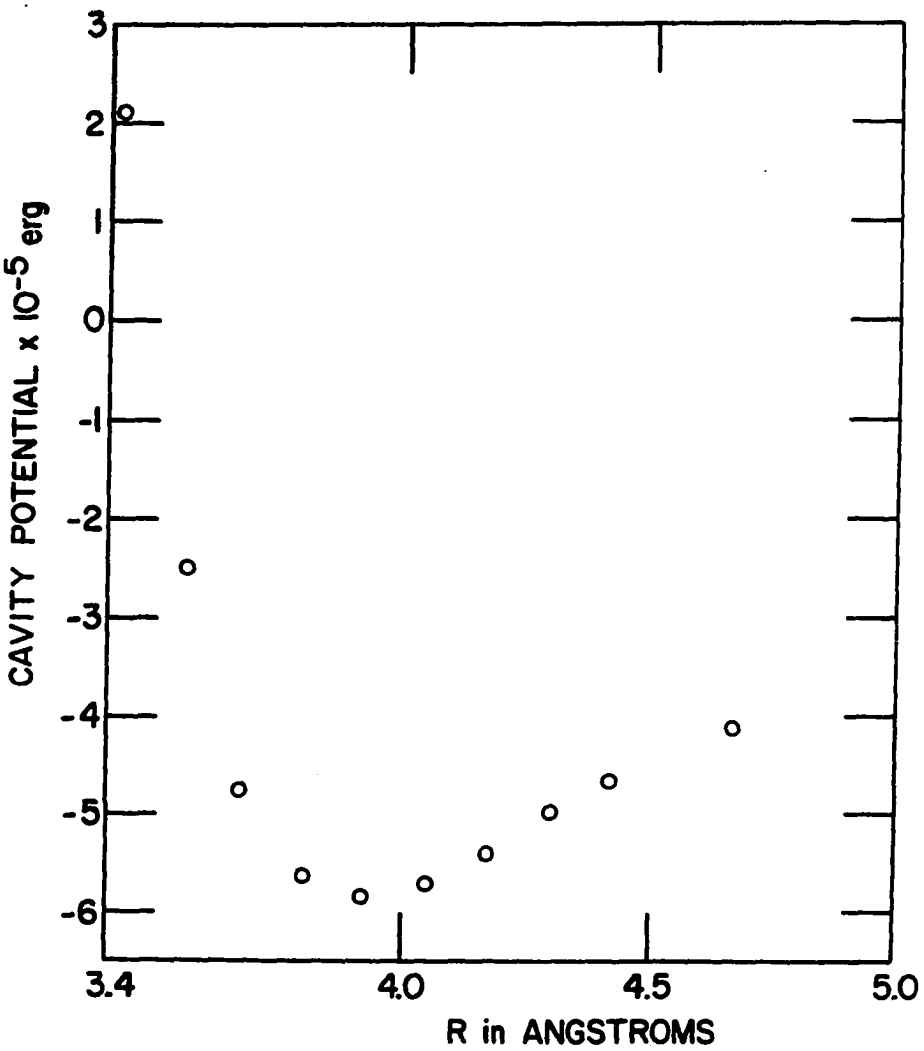

Fig. III.D.2. The lowest value of the total matrix potential as a function of the cavity size

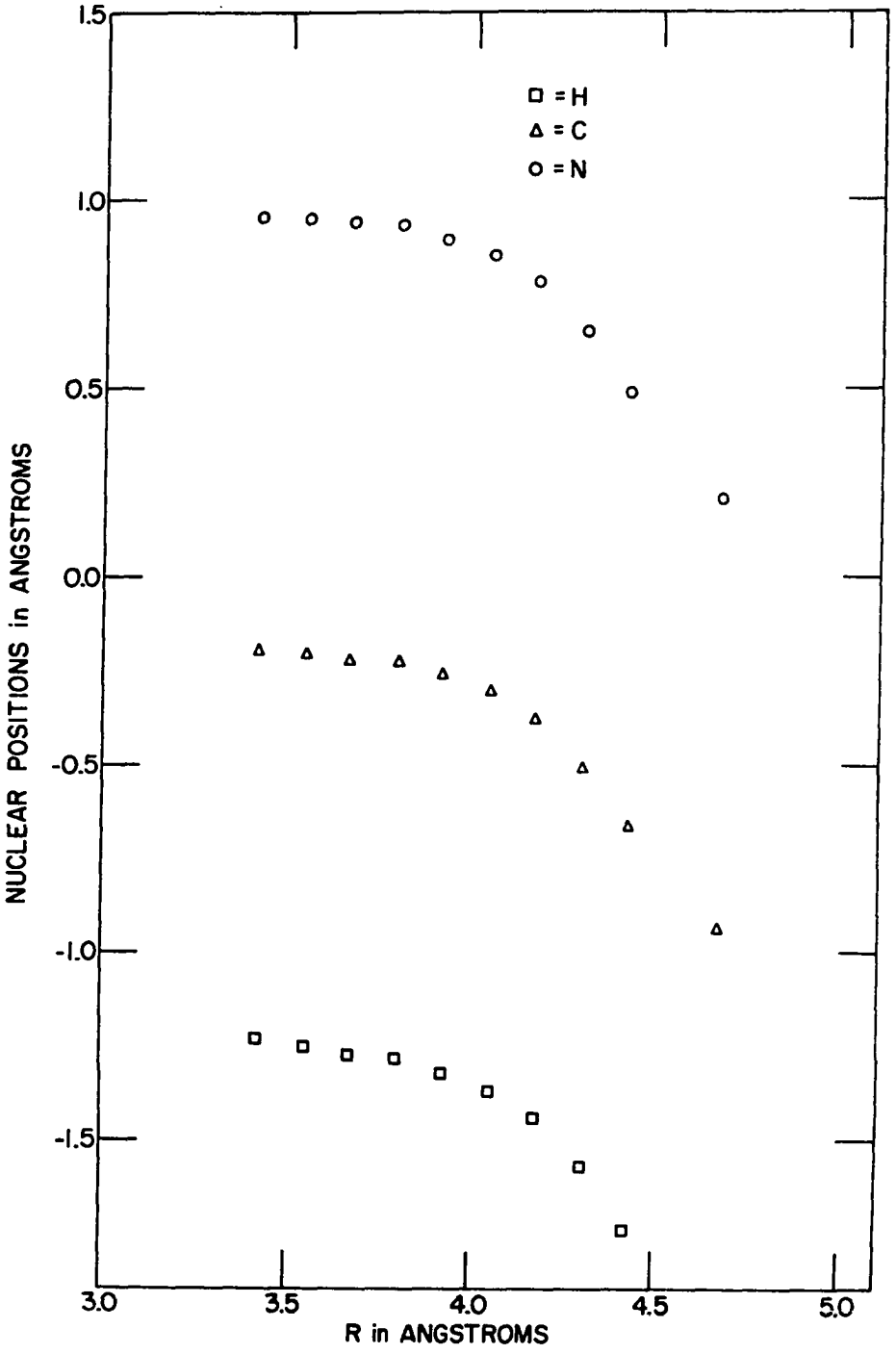

Fig. III.D.3. Positions of the H,C, and N atoms as a function of cavity size

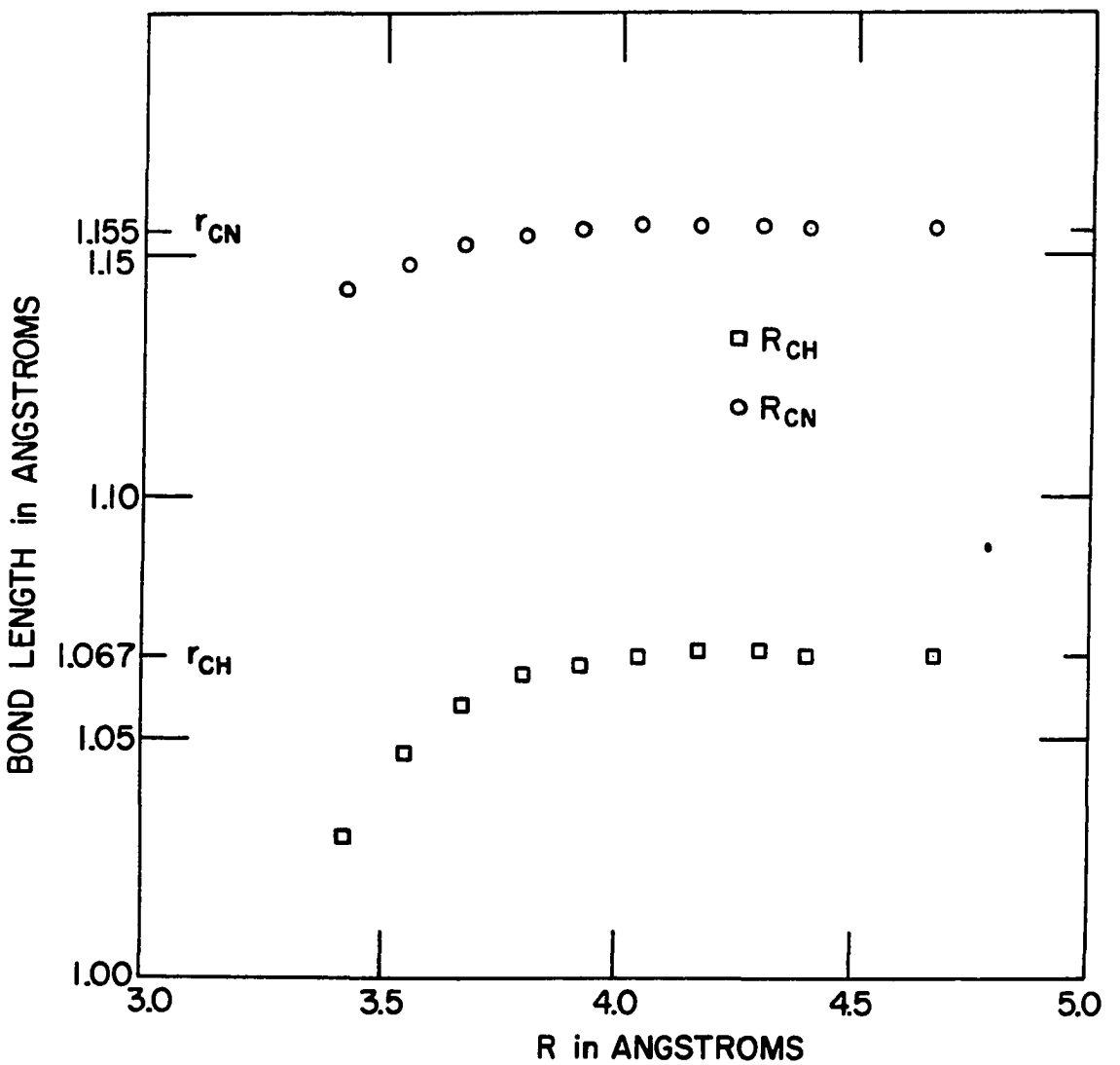

Fig. III.D.4. The r_{CN} and r_{CH} equilibrium bond lengths as a function of cavity size

E. A Vibrational Model for Molecules Trapped in Rare Gas Matrices

In the previous sections it was shown that the linear XYZ vibrational model was an inadequate description of HCN in an argon matrix. In this section a model is presented which is a better representation of the vibrational spectrum of matrix isolated HCN.

1. Diatomic model

The model will first be presented for a diatomic molecule because of the simpler algebra involved. Fig. III.E.1a shows the model for a heteronuclear diatomic molecule. The model presumes that the interaction of the cavity with the molecular system can be described by an extended molecule with intermolecular force constants f_1 and f_2. The mass contribution from the cavity, M, combines with the molecule to produce a system with linear symmetry.

The quantitative aspects of the model are developed in Appendix D. The results for the stretching frequency given by Eq. VI D.3 for the diatomic molecule is:

$$\lambda_2^m = f_2^m(\mu_X + \mu_Y) + f_1\mu_X^2/(\mu_X + \mu_Y) + f_3\mu_Y^2/(\mu_X + \mu_Y) + A + B + C + D \qquad \text{(III.E.1)}$$

where f_2^m is the force constant for the stretching of the diatomic molecule in the matrix, μ_X and μ_Y are the reciprocals of the masses of atoms X and Y, and A, B, C, and D are terms which describe the coupling of the molecule XY with the matrix.

The change in the force constant in the matrix from the value for a free diatomic molecule depends on two effects, the first is whether the diatomic system accepts or donates charge to the matrix (35,p.10). The second effect is the size of the cavity. In the former, $f_2^m > f_2^g$; when charge is taken from the cavity and $f_2^m < f_2^g$ when charge is donated to the cavity.

The second effect is due to the size of the cavity which causes $f_2^m > f_2^g$ for a tight cavity, that is when the guest is large compared to the rare gas atom, and $f_2^m \approx f_2^g$ for a loose cavity, that is when the guest is small compared to the rare gas atom. Separation of the two effects is difficult because both operate simultaneously.

In view of the above considerations one expects a different force constant in the matrix and a positive contribution to λ_2^m as the rare gas is changed from Ne to Xe because f_1 and f_3, the intermolecular force constants, increase from Ne to Xe.

Eq. III.E.1 reflects the importance of mass considerations in determining the vibrational spectrum in the matrix. For example, if the diatomic system is HBr where X = H and Y = Br, then in Eq. III.E.1 the term $f_3\mu_Y^2/(\mu_X + \mu_Y)$ becomes very small. Thus the intermolecular interactions are determined by the hydrogen cavity interaction.

2. Triatomic models

Fig. III.E.1b shows the model for HCN in an argon matrix. The f_1 and f_4 are intermolecular force constants, f_{CH}^m, f_{rr}^m, and f_{CN}^m are the HCN force constants in the matrix and M refers to a mass contribution from the argon cavity. A term by term analysis of the eigenvalues for the

stretching vibrations reveals that terms involving motions of the mass M are negligible so that the CH stretching vibration of HCN in an argon matrix is given by Eq. VI.D.11:

$$\lambda_{CH}^{m} = f_{CH}^{m}(\mu_H + \mu_C) + f_1 \mu_H^2/(\mu_H + \mu_C) - f_{rr}^{m}\mu_C \qquad \text{(III.E.2)}$$

where f_{CH}^{m} is the CH stretching force constant and f_1 is the intermolecular interaction of the hydrogen atom with the cavity. The last term in Eq. VI.D.11 has been neglected because it is small compared to the other terms.

Eq. VI.D.13 gives for the CH stretch in the gas phase:

$$\lambda_{CH}^{g} = f_{CH}^{g}(\mu_H + \mu_C) - f_{rr}^{g}\mu_C \qquad \text{(III.E.3)}$$

Hence the change in the vibrational eigenvalue upon hydrogen to deuterium isotopic substitution is:

$$\lambda_{CH}^{g} - \lambda_{CH}^{'g} = f_{CH}^{g}(\mu_H - \mu_D) \qquad \text{(III.E.4)}$$

$$\lambda_{CH}^{m} - \lambda_{CH}^{'m} = f_{CH}^{m}(\mu_H - \mu_D) + f_1[\mu_H^2/(\mu_H + \mu_C) - \mu_D^2/(\mu_D + \mu_C)] \qquad \text{(III.E.5)}$$

and for the C^{12} to C^{13} isotopic substitution:

$$\lambda_{CH}^{g} - \lambda_{CH}^{'g} = f_{CH}(\mu_{C12} - \mu_{C13}) - f_{rr}^{g}(\mu_{C12} - \mu_{C13}) \qquad \text{(III.E.6)}$$

and

$$\lambda^{m}_{CH} - \lambda'^{m}_{CH} = f^{m}_{CH}(\mu_{C12} - \mu_{C13}) - f^{m}_{rr}(\mu_{C12} - \mu_{C13})$$
$$+ f_1[\mu^2_H/(\mu_H + \mu_{C12}) - \mu^2_H/(\mu_H + \mu_{C13})] \qquad \text{(III.E.7)}$$

The isotopic shifts in the matrix and gas can be compared by defining

$$\Delta'_i = (\Delta^m_i - \Delta^g_i)$$

where

$$\Delta^m_i = \lambda^m_i - \lambda'^m_i$$

and

$$\Delta^g_i = \lambda^g_i - \lambda'^g_i$$

The quantity Δ'_i is a measure of the isotopic discrepancy between the gas and matrix. Therefore for H-D isotopic substitution

$$\Delta'_3(H,D) = (f^m_{CH} - f^g_{CH})(\mu_H - \mu_D) + f_1[\mu^2_H/(\mu_H + \mu_C) - \mu^2_D/$$
$$(\mu_D + \mu_C)] \qquad \text{(III.E.8)}$$

and for C^{12}-C^{13} isotopic substitution

$$\Delta'_3(C^{12},C^{13}) = (f^m_{CH} - f^g_{CH})(\mu_{C12} - \mu_{C13}) - (f^g_{rr} - f^m_{rr})(\mu_{C12} - \mu_{C13})$$
$$+ f_1[\mu^2_H/(\mu_H + \mu_{C12}) - \mu^2_H/(\mu_H + \mu_{C13})] \qquad \text{(III.E.9)}$$

It is to be noted that even if the force field of the guest molecule in the matrix and gas is identical, the isotope shifts will still differ due to the last term in Eqs. III.E.8 and III.E.9.

In Eq. III.E.8 the last term is positive while experimentally, $\Delta_3' < 0$; consequently, $f^m_{CH} < f^g_{CH}$. On the other hand, while the last term in Eq. III.E.9 for the CH stretch contributes a small negative quantity to Δ_3' the first term dominates. Thus, the net result is $\Delta_3'(C^{12},C^{13}) << \Delta_3'(H,D)$ because the right hand side of Eq. III.E.9 is multiplied by a small term $\mu_{C12} - \mu_{C13}$. This agrees with the experimental observation shown in Table III.A.4.

Similar analysis for the CN stretching frequency in the matrix yields,

$$\lambda^m_{CN} = f^m_{CN}(\mu_C + \mu_N) - \mu_C f^m_{rr} + f_4\mu_N^2/(\mu_C + \mu_N) \qquad \text{(III.E.10)}$$

and in the gas phase,

$$\lambda^g_{CN} = f^g_{CN}(\mu_C + \mu_N) - \mu_C f^g_{rr} \qquad \text{(III.E.11)}$$

Thus for N^{14} to N^{15} isotopic substitution,

$$\Delta_1'(N^{14},N^{15}) = (f^m_{CN} - f^g_{CN})(\mu_{N14} - \mu_{N15}) - f_4[\mu^2_{N14}/(\mu_{C12} - \mu_{N14}) - \mu^2_{N15}/(\mu_{C12} - \mu_{N15})] \qquad \text{(III.E.12)}$$

The change of the curvature of the potential function at the minimum in the matrix relative to the gas cannot be determined accurately because the small solvent shifts are within experimental error. This is consonant with Eq. III.E.12 which predicts a small effect because of the heavier masses involved.

The eigenvalue for the bending mode of HCN in the model is given by Eq. VI.D.17:

$$\lambda_\theta^m = f_\theta^m A - f_1 B^2/A - f_2 C^2/A \qquad \text{(III.E.13)}$$

while for the gas phase Eq. VI.D.21 gives,

$$\lambda_\theta^g = f_\theta^g A \qquad \text{(III.E.14)}$$

where

$$A = \mu_H/r_{CH}^2 + \mu_C(1/r_{CH} + 1/r_{CN})^2 + \mu_N/r_{CN}^2 \qquad \text{(III.E.15)}$$

$$B = \mu_C(1/r_1 + 1/r_{CH})/r_{CH} + \mu_C(1/r_{CH} + 1/r_{CN})/r_{CH} \qquad \text{(III.E.16)}$$

$$C = \mu_C(1/r_{CH} + 1/r_{CN})/r_{CN} + \mu_N(1/r_{CH} + 1/r_4)/r_{CN} \qquad \text{(III.E.17)}$$

In these expressions, f_θ^m and f_θ^g are the matrix and gas phase bending force constants for HCN, f_1 and f_3 are bending force constants for the M-H-C and C-N-M angles, (See Fig. III.E.1c), r_1, r_4 are the internuclear distances for the matrix-hydrogen and nitrogen-matrix distances are r_{CH}, r_{CN} are the gas phase CH and CN equilibrium bond lengths.

For H-D isotopic substitution:

$$\Delta_2'(H,D) = (f_\theta^m - f_\theta^g)(\mu_H - \mu_D)/r_{CH}^2 \qquad \text{(III.E.18)}$$

where the second and third terms are negligible compared to the first term in Eq. III.E.13.

Similarly for C^{12} to C^{13} isotopic substitution,

$$\Delta_2'(C^{12},C^{13}) = (f_\theta^m - f_\theta^g)(\mu_{C12} - \mu_{C13})(1/r_{CH} + 1/r_{CN})^2 \qquad \text{(III.E.19)}$$

and for N^{14} to N^{15} isotopic substitution,

$$\Delta_2'(N^{14},N^{15}) = (f_\theta^g - f_\theta^m)(\mu_{N^{14}} - \mu_{N^{15}})/r_{CN}^2 \qquad \text{(III.E.20)}$$

Consideration of the differences in the isotopic masses in Eqs. III.E.18, III.E.19, and III.E.20 predicts,

$$\Delta_2'(C^{12},C^{13}) \text{ and } \Delta_2'(N^{14}, N^{15}) << \Delta_2'(H,D)$$

as found in Table III.A.4. Since the terms involving mass and geometry in Eq. III.E.20 are positive and $\Delta_2'(H,D) > 0$ then $f_\theta^m > f_\theta^g$.

Summarizing the above results, Δ_i', the difference between the matrix and gas phase isotopic frequencies can be explained by a change in curvature of the potential function at the minimum. The size of the effect on the isotopic frequencies is governed by the magnitude of the masses involved. Hence, the large isotopic mass differences for H-D substitution magnifies the isotopic discrepancies while small isotopic mass differences tend to cause small isotopic discrepancies.

The implications of this result in matrix isolation structure determination is as follows: The spherical cell model has shown that a rare gas matrix causes a negligible effect on geometry while in this section it is shown that the matrix isotopic discrepancies are created by a combination of mass and potential curvature effects. Thus, whenever a pair of isotopic frequencies are used to determine molecular geometry, Δ_i', the isotopic discrepancy must be less than experimental error. If not, the matrix isotopic discrepancies will be falsely attributed to a change in geometry. This criterion will not likely be met for light isotopes since frequency accuracy of the order of 0.1 cm^{-1} is required for reliable geometries in the matrix.

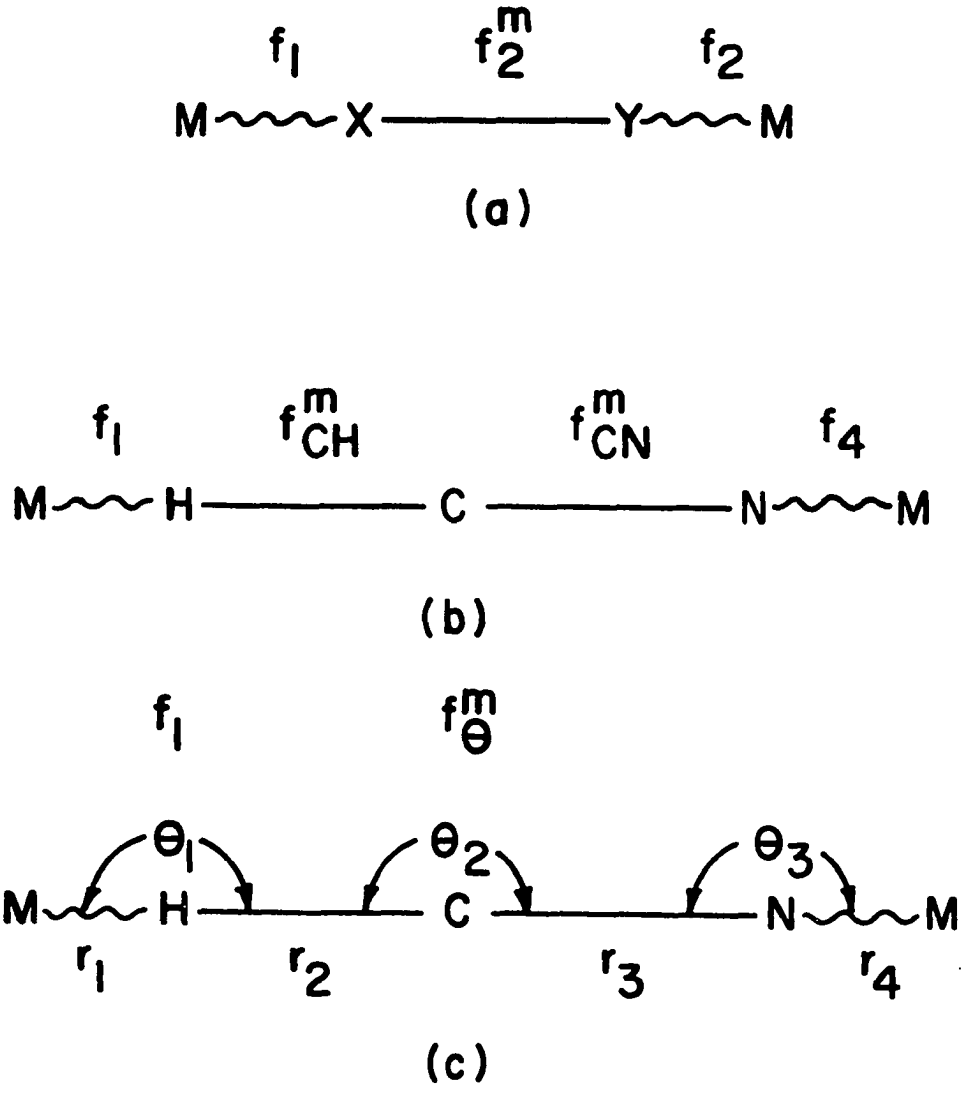

Fig. III.E.1. Matrix models: (a) diatomic model, (b) stretching modes for the triatomic matrix model, (c) bending modes for the triatomic matrix model

F. Matrix Frequency Shifts in the HCN Spectrum

In this section a simple empirical model for isolating the relative contributions of geometry changes, force constant changes and anharmonic changes to the curve is constructed. If the valence coordinates are essentially normal coordinates, comparison of potential curves for a molecule in the gas phase and a solvent shows the following possible changes which are schematically depicted in Fig. III.F.1 for a diatomic molecule.

First, the solvent can cause a change in the bond length, so that the potential curve for the bond in the solvent is shifted along the abscissa (Fig. III.F.1b).

Second, a change in curvature of the potential function for the bond at the equilibrium configuration can occur, that is the bond force constant can change (Fig. III.F.1c).

Third, anharmonicities for the bond in the solvent environment can change without a change in the bond force constant. This effect causes a decrease in the spacing between successive energy levels if the anharmonicity increases.

In reality all the effects exist simultaneously, however, in some cases the magnitude of the effects can be determined to reveal their relative importance. An examination of the three effects for HCN has shown that the geometry and anharmonicity changes are insignificant but that changes in curvature, although small, are important.

The relative importance of the three possible changes on matrix shifts can be considered by writing equations for matrix shifts derived in

Appendix D. Consider Eq. VI.D.15 for the CH matrix shift,

$$\lambda^{g}_{CH} - \lambda^{m}_{CH} = (f^{g}_{CH} - f^{m}_{CH})(\mu_H - \mu_C) + (f^{m}_{rr} - f^{g}_{rr})\mu_C - f_1\mu_H^2/(\mu_H + \mu_C) \qquad \text{(III.F.1)}$$

and Eq. VI.D.16 for the CN matrix shift,

$$\lambda^{g}_{CN} - \lambda^{m}_{CN} = (f^{g}_{CN} - f^{m}_{CN})(\mu_C + \mu_N) + (f^{m}_{rr} - f^{g}_{rr})\mu_C - f_4\mu_N^2/(\mu_C + \mu_N) \qquad \text{(III.F.2)}$$

Since

$$\lambda_i = 4\pi^2c^2\omega_i^2/N_a = K\omega_i^2$$

and

$$\omega_i = \nu_i/(1 - \alpha_i)$$

Eqs. III.F.1 and III.F.2 can be written:

$$[\nu^{g}_{CH}/(1 - \alpha^{g}_{CH})]^2 - [(\nu^{m}_{CH}/(1 - \alpha^{m}_{CH})]^2 = \qquad \text{(III.F.3)}$$

$$[(f^{g}_{CH} - f^{m}_{CH})(\mu_H + \mu_C) + (f^{m}_{rr} - f^{g}_{rr})\mu_C - f_1\mu_H^2/(\mu_H + \mu_C)]/K$$

and

$$[\nu^{g}_{CN}/(1 - \alpha^{g}_{CN})]^2 - [\nu^{m}_{CN}/(1 - \alpha^{m}_{CN})]^2 = \qquad \text{(III.F.4)}$$

$$[(f^{g}_{CN} - f^{m}_{CN})(\mu_C + \mu_N) + (f^{m}_{rr} - f^{g}_{rr})\mu_C - f_4\mu_N^2/(\mu_C + \mu_N)]/K$$

These equations show that the matrix shifts depend both on anharmonicities and changes in curvature of the potential function. In

this case a change in bond length has no effect on the matrix shift. Their relationship can be found by supposing the bonds in a polyatomic molecule act like diatomic molecules and that an unspecified parameter Y is responsible for the perturbation of the gas phase potential. Differentiation of the expression

$$\nu = \omega(1 - \alpha)$$

with respect to Y gives

$$\partial\alpha/\partial Y = [(1 - \alpha)\partial\omega/\partial Y - \partial\nu/\partial Y]/\omega \qquad \text{(III.F.5)}$$

Since

$$\omega = (N_a f/\mu)^{1/2}/2\pi c \qquad \text{(III.F.6)}$$

substitution of Eq. III.F.6 into Eq. III.F.5 gives

$$\partial\alpha/\partial Y = [(N_a/\mu f)^{1/2}(1 - \alpha)/4\pi c)\partial f/\partial Y - \partial\nu/\partial Y]/ \qquad \text{(III.F.7)}$$

unless the matrix shift is nearly zero, that is $\partial\nu/\partial Y \approx 0$, the first term on the right hand side of Eq. III.F.7 is small compared to $\partial\nu/\partial Y$ hence:

$$\partial\alpha/\partial Y \approx -(1/\nu)\partial\nu/\partial Y \qquad \text{(III.F.8)}$$

Therefore a matrix shift to a lower frequency is associated with increasing anharmonicity and matrix shifts to higher frequencies is associated with decreasing anharmonicity.

Applying these considerations to the CH bond where $\omega \approx 3441$ cm^{-1}

$f = 6.2$, $\partial f/\partial Y \approx -0.1$, $\partial \nu/\partial Y = -6.0$, Eq. III.F.7 gives $\partial \alpha/\partial Y \approx 0.001$, a very small increase in anharmonicity. Similarly for the CN bond $\partial \alpha/\partial Y \approx 0$. Hence, this simple treatment agrees with the experimental observation in the previous section that anharmonicity changes contribute very little to HCN matrix shifts.

The effect of mass on the matrix shift is very important because large masses make all the terms in Eqs. III.F.3 and III.F.4 small and tend to produce small anharmonic contributions to the matrix shifts while the opposite is true for small masses.

Another important consideration of Eq. III.F.3 and Eq. III.F.4 is the combined effect of the intermolecular force constants to produce shifts. Shifts to higher frequencies are produced in environments where $f^m \gg f^g$, consequently, the small matrix shifts observed for the CN stretch may be primarily due to the f_4 term in Eq. III.F.6 if $f^m_{CN} \approx f^g_{CN}$. For the CH stretch it has already been shown that $f^m_{CH} < f^g_{CH}$ giving an observed shift to lower frequency thus, $(f^g_{CH} - f^m_{CH}) > f_1$.

The matrix shift for the bending mode is given by Eq. VI.D.22.

$$\lambda^g_\theta - \lambda^m_\theta = (f^g_\theta - f^m_\theta)A - f_1 B^2/A - f_2 C^2/A \qquad \text{(III.F.9)}$$

where Eqs. VI.D.18 to VI.D.20 define A, B, and C. Substituting the anharmonicity into Eq. III.F.9 one obtains

$$[\nu^g_\theta/(1 - \alpha^g_\theta)]^2 - [\nu^m_\theta/(1 - \alpha^m_\theta)]^2 =$$

$$[(f^g_\theta - f^m_\theta)A - f_1 B^2/A - f_2 C^2/A]/K \qquad \text{(III.F.10)}$$

In Eq. III.F.10 the contribution due to f_1 and f_2 are small because B^2 and C^2 are very small. The A term may be reduced to give the following expression for the matrix shift:

$$[\nu_\theta^g /(1 - \alpha_\theta^g)] - (\nu_\theta^m /(1 - \alpha_\theta^m)] =$$

$$[(f_\theta^g - f_\theta^m)\mu_H/r_{CH}^2]/K \qquad \text{(III.F.11)}$$

Previously, it was shown that anharmonicity changes for the bending mode were small and $f_\theta^m > f_\theta^g$; therefore the shift to higher frequency in the bending mode is due to a combined effect of the increased curvature in the potential function which is amplified by the small mass of the hydrogen atom. This increased curvature is due to an interaction of the hydrogen with the neighboring argon atoms.

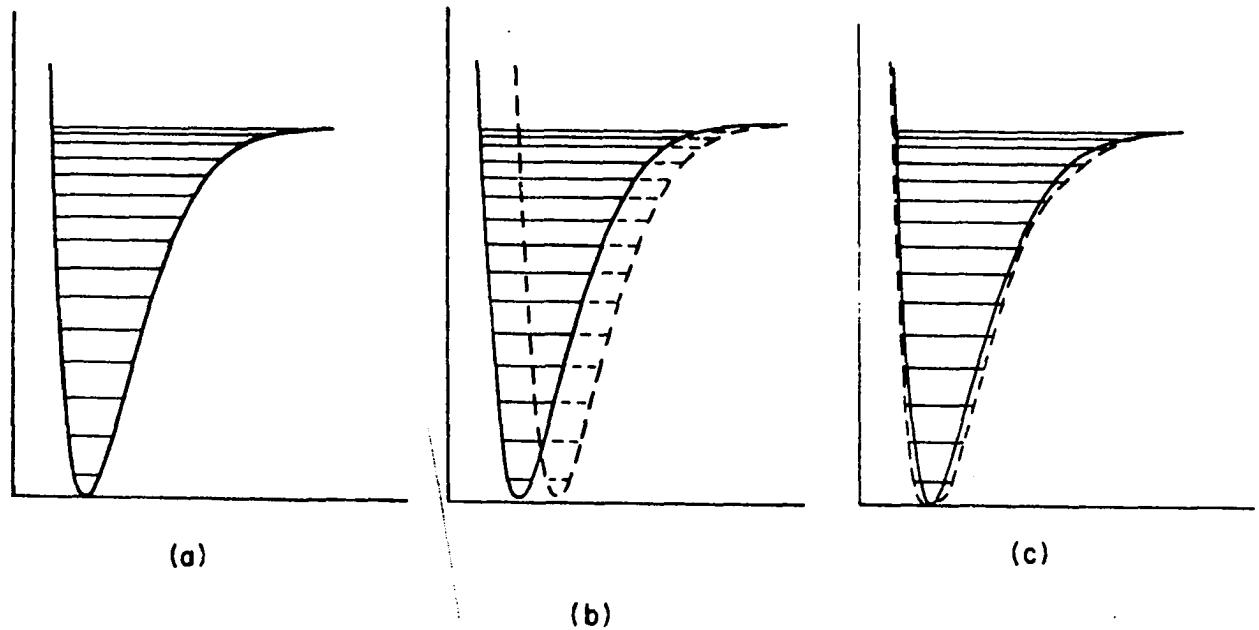

Fig. III.F.1. Possible matrix effects on the potential function: (a) gas phase potential as a function of bond length, (b) dotted line shows the effect of a change in bond length, (c) dotted line shows the effect of a change in the force constant

IV. LITERATURE CITED

1. Allavena, M., Rysnik, R., White D., Calder, V., and Mann, D. E., J. Chem. Phys., 50, 3399 (1969).

2. Allen, H. C., and Plyler, E. K., J. Chem. Phys., 25, 1132 (1956).

3. Allen, H. C., Plyler, E. K., and Blaine, L. R., J. Res. NBS, 59, 211 (1957).

4. Barnes, A. J. and Hallman, H. E., Quarterly Reviews, 23, 393 (1969).

5. Bernstein, H. J., Spectrochim. Acta, 18, 161 (1962).

6. Bratoz, S., J. Chem. Phys., 23, 159 (1955).

7. Burns, C. A. and Gordy, W., Phys. Rev., 101, 599 (1956).

8. Calder, V., Mann, D. E., Seshadri, K. S., Allavena, M., and White, D., J. Chem. Phys., 51, 2093 (1969).

9. Checkland, P. B. and Thompson, H. W., Trans. Faraday Soc., 51, 1 (1955).

10. Christensen, D. H. and Nielsen, O. F., J. Mol. Spectrosc., 33, 425 (1970).

11. Dennison, D. M., J.O.S.A., 50, 1267 (1960).

12. Duncan, J. L. and Mills, I. M., Spectrochim. Acta, 20, 523 (1964).

13. Edgell, W. F. and Riethof, T. R., J. Phys. Chem., 56, 326 (1942).

14. Edwards, T. H. and Willson, P. D., and Degler, W. D., J.O.S.A., 59, 496 (1969).

15. Edwards, T. H., Moncur, N. K., and Synder, L. E., J. Chem. Phys., 46, 2139 (1970).

16. Fraley, P. and Rao, K., J. Mol. Spectrosc., 26, 312 (1969).

17. Gamo, I., J. Mol. Spectrosc., 30, 316 (1969).

18. Herzberg, G., Molecular Spectra and Molecular Structure II. Infrared and Raman Spectra of Polyatomic Molecules, (D. Van Nostrand Co., Inc., Princeton, N. J. 1945).

19. Hillger, R. E. and Strandberg, M.W.P., Phys. Rev., 83, 575 (1951).

20. Hoffman, R. E. and Hornig, D. F., J. Chem. Phys., 17, 1163 (1949).

21. Hyde, G. E. and Hornig, D. F., J. Chem. Phys., 20, 647 (1952).

22. Jacox, M. E. and Milligan, D. E., Appl. Optics, 8, 873 (1964).

23. Maki, A. G., J. Chem, Phys., 35, 931 (1961).

24. Mann, D. E., Calder, G. V., Seshadri, K. S., White, D., and Linevsky, M. J., J. Chem, Phys., 46, 1138 (1967).

25. Miller, R. E. and Eggers, D. F., J. Chem. Phys., 45, 3028 (1966).

26. Miller, R. E., Leroi, G. E. and Eggers, D. F., J. Chem. Phys., 46, 2139 (1967).

27. Mills, I. M., J. Mol. Spectrosc., 5, 334 (1960).

28. Nakagawa, T. and Morino, Y., Bull, Chem. Soc. Jap., 42, 2212 (1969).

29. Nibler, J. W. and Pimentel, G. C., J. Mol. Spectrosc., 26, 294 (1968).

30. Oka, T. and Morino, Y., J. Mol. Spectrosc., 8, 9 (1962).

31. Pacansky, J. and Calder V., J. Chem. Phys., 53, 4519 (1970).

32. Pimentel, G. C. and Charles, S. W., Pure Appl. Chem., 7, 111 (1963).

33. Phyler, E. K., Danti, A., Blaine, L. R. and Tidwell, E. D., Nat. Bur. of Standards Monograph 16 (1960).

34. Rao, K. N., Humphreys, C. J. and Rank, D. H., Wavelength Standards in the Infrared, (Academic Press Inc., New York, 1966).

35. Robinson, G. W., Advances in Chemistry Series, No. 36, (American Chemical Society, Washington D. C., 1962).

36. Saito, S., J. M. Spectrosc., 30, 1 (1969).

37. Shelton, R. D., Nielson, A. H. and Fletcher, W. F., J. Chem. Phys., 21, 2178 (1968).

38. Simmons, J. W., Anderson, W. E. and Gordy, W., Phys. Rev., 86, 1055 (1952).

39. Synder, L. E. and Edwards, T. H., J. Mol. Spectrosc., 31, 347 (1969).

40. Wilson, E. B., Jr., Decius, J. C. and Cross P. C., Molecular Vibrations, (McGraw Hill Book Co. Inc., New York, 1955).

V. ACKNOWLEDGEMENT

I am indebted to my research advisor, Dr. G.V. Calder, for making my research possible. I am also indebted to my good friend, Abe Malae, for typing my thesis.

Most of all, I am indebted to Nancy, Ginette, and Michelle whose patience and understanding made my work possible.

VI. APPENDICES

A. Solution of a Secular Determinant by Perturbation Theory

The expanded secular determinant is

$$\begin{vmatrix} H_{11}-\lambda & H_{12} & \cdot & \cdot & H_{1n} \\ H_{21} & H_{22}-\lambda & 0 & \cdot & 0 \\ \cdot & \cdot & \cdot & & \cdot \\ \cdot & \cdot & & \cdot & \cdot \\ H_{n1} & 0 & \cdot & & H_{nn}-\lambda \end{vmatrix} = 0$$

The first order approximation for the t^{th} eigenvalue is

$$\lambda_t = H_{tt} \qquad \text{(VI.A.1)}$$

The second order approximation is found by replacing the exact secular determinant with

$$\begin{vmatrix} H_{11}-\lambda & H_{12} & \cdot & \cdot & H_{1n} \\ H_{21} & H_{22}-H_{11} & \cdot & \cdot & 0 \\ \cdot & \cdot & \cdot & & \cdot \\ \cdot & \cdot & & \cdot & \cdot \\ H_{n1} & 0 & \cdot & & H_{nn}-H_{11} \end{vmatrix} = 0$$

The λ's which should appear in the second, third, etc., diagonal terms are replaced by the first order approximation for λ_1, that is, $\lambda_1 = H_{11}$. The second order approximation is justified provided $H_{tt} - H_{ii} (t \neq i)$ are large, and is appropriate in that the neglected off diagonal

terms can only affect the desired λ indirectly.

The approximate secular determinant is solved by multiplication of each i^{th} row by $H_{ii}/(H_{ii} - H_{11})$ and a subsequent subtraction from the first row. In this manner the secular determinant is transformed to the following form:

$$[(H_{11} - \lambda) - \sum_{t=1}^{n} H_{1t}H_{t1}/(H_{tt} - H_{11})](H_{22} - H_{11})(H_{33} - H_{11}) \ldots (H_{nn} - H_{11}) = 0$$

Consequently, λ , approximated to the second order is

$$\lambda_1 = H_{11} - \sum H_{1t}H_{t1}/(H_{tt} - H_{11}) \qquad \text{(VI.A.2)}$$

or for any other $\lambda_{t'}$:

$$\lambda_{t'} = H_{t't'} - \sum_{t \neq t'} H_{tt'}H_{t't}/(H_{tt} - H_{t't'}) \qquad \text{(VI.A.3)}$$

The unnormalized eigenvector $L_{t't}$, obtained through a solution of the approximate secular determinant is

$$L_{t't} = [H_{tt'}/(H_{t't'} - H_{tt})]L_{t't'} \qquad \text{(VI.A.4)}$$

where $L_{t't'} = 1$ and $t \neq t'$.

B. $\tilde{F}$, $\tilde{G}$, $\tilde{H} = \tilde{F}\tilde{G}$ Elements for a Bent, Symmetric, Triatomic Molecule

The molecular parameters for a bent, symmetric, triatomic molecule are shown in Fig. VI.B.1 where α is the equilibrium bond angle, and r is the equilibrium bond length.

The matrices $\tilde{F}$, $\tilde{G}$, and $\tilde{H} = \tilde{F}\tilde{G}$ are 3 x 3 matrices whose elements are

functions of the molecular parameters are given below:

$$F_{11} = f_r + f_{rr}$$

$$F_{22} = r_e^2 f_\alpha$$

$$F_{33} = f_r - f_{rr}$$

$$F_{12} = F_{21} = 2^{1/2} r_e f_{r\alpha}$$

$$F_{13} = F_{31} = F_{23} = F_{32} = 0$$

$$G_{11} = \mu_X(1 + \cos\alpha) + \mu_Y$$

$$G_{22} = 2\mu_Y/r_e^2 + (2\mu_X/r_e^2)(1 - \cos\alpha)$$

$$G_{33} = \mu_X(1 - \cos\alpha) + \mu_Y$$

$$G_{12} = G_{21} = - 2^{1/2}/r_e \mu_Y \sin\alpha$$

$$G_{13} = G_{31} = G_{23} = G_{32} = 0$$

$$H_{11} = F_{11}G_{11} + F_{12}G_{12}$$

$$H_{22} = F_{22}G_{22} + F_{12}G_{12}$$

$$H_{33} = F_{33}G_{33}$$

$$H_{12} = F_{11}G_{12} + F_{12}G_{22}$$

$$H_{21} = F_{22}G_{12} + F_{12}G_{11}$$

$$H_{13} = H_{31} = H_{23} = H_{32} = 0$$

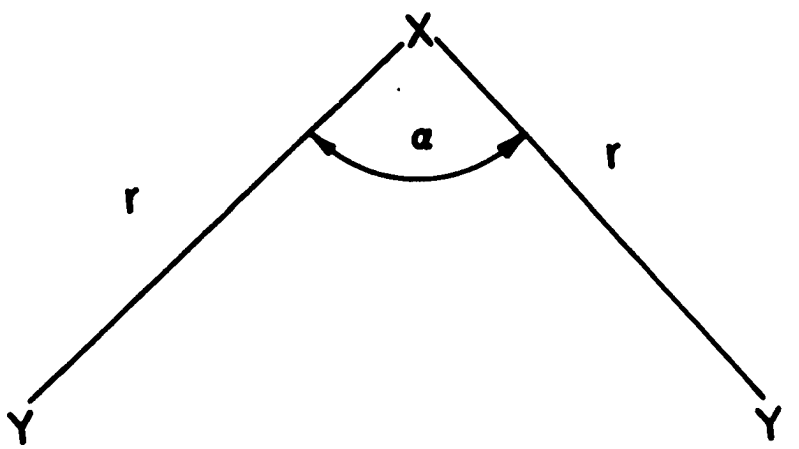

Fig. VI.B.1. The bent, symmetric triatomic model

In these equations μ_X, μ_Y and $r_e = r_1 = r_2$ refer to the reciprocal of the masses of the atoms X and Y in atomic mass units and the equilibrium internuclear separation, in A, respectively.

C. The Spherical Cell Model for HCN in an Argon Matrix

The assumptions used to construct the spherical model are: first, an HCN molecule is isolated in an argon environment with a face centered cubic symmetry; second, only the H and N ends of the HCN molecule interact with argon atoms; third, the Ar-H, Ar-N interactions are given by the usual Lennard-Jones 6-12 potential where the potential is averaged over the surface of sphere.

Fig. VI.C.1 shows the spherical model for an Ar-H or Ar-N interaction where R is the radius of the spherical cavity, a is the distance from the atom considered to the center of the cavity and r is the distance from the center of the atom in consideration to an Ar atom whose center lies on the surface of a sphere.

Since the Ar atoms are assumed to be smeared over the surface of a sphere then the average potential is,

$$\psi(a,R) = 1/4\pi \int d\underline{R}\, \phi(\underline{r}) \qquad \text{(VI.C.1)}$$

From the law of cosines,

$$r = (R^2 + a^2 + 2aR\cos\theta)^{1/2} \qquad \text{(VI.C.2)}$$

which substituted into Eq. VI.C.1 gives

$$\psi(a,R) = 1/2\int_{-1}^{1} d(\cos\theta)\ [(R^2 + a^2 + 2aR\cos\theta)^{1/2}] \qquad \text{(VI.C.3)}$$

letting $X = \cos\theta$,

$$\psi(a,R) = 1/2\int_{-1}^{1} dX\ [(R^2 + a^2 + 2aRX)^{1/2}] \qquad \text{(VI.C.4)}$$

and

$$Y = R^2 + a^2 + 2aRX \qquad \text{(VI.C.5)}$$

then

$$dY = 2aRdX \qquad \text{(VI.C.6)}$$

Substitute Eqs. VI.C5 and VI.C.6 into VI.C.4 with the Lennard-Jones potential:

$$\phi(Y) = 4\epsilon[(\sigma/Y)^{12} - (\sigma/Y)^6] \qquad \text{(VI.C.7)}$$

one obtains,

$$\psi(a,R) = \epsilon/aR\int_{(R-a)^2}^{(R+a)^2} dY[(\sigma^2/Y)^6 - (\sigma^2/Y)^3] \qquad \text{(VI.C.8)}$$

Integration gives the spherically averaged potential for an Ar-atom interaction, which for Ar-H is

$$\psi(a,R) = (\epsilon\sigma^2/aR)[1/2((\sigma/(R + a))^4 - (\sigma/(R - a)^4)$$

$$- 1/5((\sigma/(R + a))^{10} - (\sigma/(R - a))^{10}] \qquad \text{(VI.C.9)}$$

Since there are n_1 nearest neighbors at R_1 and n_2 next nearest neighbors at R_2 then the spherically averaged potential is

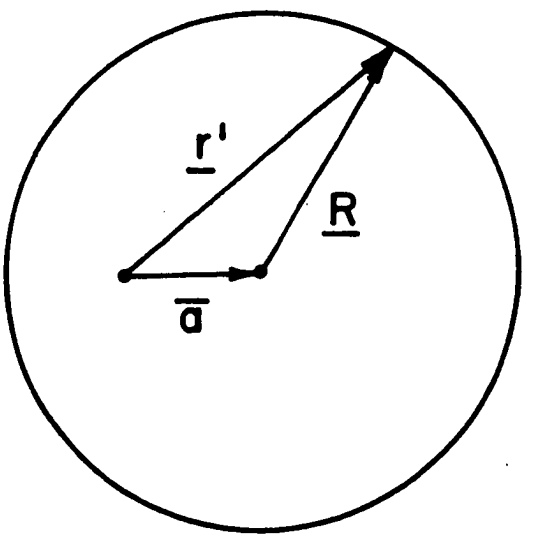

Fig. VI.C.1. The spherical cell model for an atom - argon interaction

$$\psi'(a,R) = \sum_{i=1} n_i \psi(a,R_i) \qquad \text{(VI.C.10)}$$

A similar expression exists for the Ar-N interaction,

$$\xi'(a,R) = \sum_{i=1} \xi(a,R_i) \qquad \text{(VI.C.11)}$$

Thus, the total potential energy for HCN in a spherical cavity is

$$\chi(a,b,c,R) = \sum_{i=1} n_i [\psi(a,R_i) + \xi(c,R_i)] + \phi_{CH} + \phi_{CN} \qquad \text{(VI.C.12)}$$

where

$$\phi_{CH} = f_{CH}(r_{CH} - b - a)^2/2 \qquad \text{(VI.C.13)}$$

$$\phi_{CN} = f_{CN}(r_{CN} - c - b)^2/2 \qquad \text{(VI.C.14)}$$

The r_{CH} and r_{CN} are the equilibrium CH and CN bond distances; a, b, c are the distances from the center of the cavity to the H, C, and N atoms and, ϕ_{CH} and ϕ_{CN} are the harmonic oscillator approximation for the potential energy of the CH and CN bonds.

D. Derivation of the Vibrational Model for Molecules Trapped in Rare Gas Matrices

1. Diatomic molecules

Fig. VI.D.1a shows the model for a heteronuclear diatomic molecule in rare gas matrix where M is a large mass contribution from the cavity wall, f_1, f_3 are the intermolecular force constants for the molecule-cavity interactions and f_2^m is the diatomic intramolecular force constant in the matrix.

Appendix E shows the $\tilde{F}$, $\tilde{G}$ and $\widetilde{FG}$ for the vibrational modes. The

eigenvalues for the vibrational modes are calculated by

$$\lambda_2^m = H_{22} - H_{12}H_{21}/(H_{11} - H_{22}) - H_{32}H_{23}/(H_{33} - H_{22}) \qquad \text{(VI.D.1)}$$

where $H_{ij} = (FG)_{ij}$. After substitution of the $(FG)_{ij}$ into Eq. VI.D.1:

$$\begin{aligned}\lambda_2^m = {} & f_2^m(\mu_X + \mu_Y) - \mu_X f_{12} - f_{23}\mu_Y \\ & - [f_{12}(\mu_X + \mu_Y) - f_1\mu_X][f_{12}(\mu_M + \mu_X) - f_2^m\mu_X]/ \\ & [f_1(\mu_M + \mu_X) - f_2^m(\mu_X + \mu_Y) - f_{23}\mu_Y] \qquad \text{(VI.D.2)} \\ & - [f_{23}(\mu_X + \mu_Y) - f_3\mu_Y][f_{23}(\mu_Y + \mu_M) - f_2^m\mu_Y]/ \\ & [f_3(\mu_Y + \mu_M) - f_2^m(\mu_X + \mu_Y) + f_{23}\mu_Y]\end{aligned}$$

Since $f_2^m >> f_{23}$ and f_1 then neglecting the terms in the denominator of the right hand side of Eq. VI.D.2 gives:

$$\begin{aligned}\lambda_2^m = {} & f_2^m(\mu_X + \mu_Y) - 2\mu_X f_{12} - 2f_{23}\mu_Y + f_1\mu_X^2/(\mu_X + \mu_Y) \\ & f_3\mu_Y^2/(\mu_X + \mu_Y) + A + B + C + D \qquad \text{(VI.D.3)}\end{aligned}$$

where

$$A = f_{12}^2(\mu_M + \mu_X)/f_2^m \qquad \text{(VI.D.4)}$$

$$B = f_1 f_{12}\mu_X(\mu_M + \mu_X)/[(f_2^m(\mu_X + \mu_Y)] \qquad \text{(VI.D.5)}$$

$$C = f_{23}^2(\mu_Y + \mu_M)/f_2^m \qquad \text{(VI.D.6)}$$

$$D = - f_3 f_{23}\mu_Y(\mu_Y + \mu_M)/f_2^m \qquad \text{(VI.D.7)}$$

The motion of the cavity enters into Eq. VI.D.3 through the terms A, B, C, and D which involves μ_M. A term by term analysis of A, B, C, and D reveals that these terms are very small because they contain the square of small force constants and reciprocal mass terms. This means that the kinetic effect of the cavity is negligible. Dropping the small terms from Eq. VI.D.3 the eigenvalue for the stretching mode is approximately:

$$\lambda_2^m = f_2^m(\mu_X + \mu_Y) + f_1\mu_X^2/(\mu_X + \mu_Y) + f_3\mu_Y^2/(\mu_X + \mu_Y) \qquad \text{(VI.D.8)}$$

Since the gas phase eigenvalue is

$$\lambda_2^g = f_2^g(\mu_X + \mu_Y) \qquad \text{(VI.D.9)}$$

then the matrix shift is

$$\lambda_2^m - \lambda_2^g = (f_2^g - f_2^m)(\mu_X + \mu_Y) + f_1\mu_X^2/(\mu_X + \mu_Y) + f_3\mu_Y^2/(\mu_X + \mu_Y) \qquad \text{(VI.D.10)}$$

2. Triatomic molecule (bond stretching modes)

Fig. VI.D.1b shows the model for a triatomic molecule in a cavity where M refers to a mass contribution from the cavity wall, f_1, f_4 are intermolecular potential functions, and f_2^m, f_3^m are the intramolecular potential functions for the XYZ triatomic molecule.

The $\tilde{F}$, $\tilde{G}$, and $\tilde{F}\tilde{G}$ matrix elements are listed in Appendix F. Eigenvalues for the X-Y and Y-Z stretching frequencies are found in a manner similar to those for the diatomic system. The general expressions for the XY, YZ modes are given by Eq. VI.A.3 and the matrix elements are listed in

Appendix F. In the triatomic case it is also found that the kinetic effect of the cavity is negligible. Hence, the results are for the X-Y stretch

$$\lambda_2^m = f_2^m(\mu_X + \mu_Y) - \mu_Y f_{23}^m + f_1\mu_X^2/(\mu_X + \mu_Y)$$
$$- f_2^m f_3^m \mu_Y^2/[f_3^m(\mu_Y + \mu_Z) - f_2^m(\mu_X + \mu_Y)] \qquad \text{(VI.D.11)}$$

and the Y-Z stretch:

$$\lambda_3^m = f_3^m(\mu_Y + \mu_Z) - \mu_Y f_{23}^m + f_4\mu_Z^2/(\mu_Y + \mu_Z)$$
$$- f_2^m f_3^m \mu_Y^2/[f_2^m(\mu_Y + \mu_Z) - f_3^m(\mu_X + \mu_Y)] \qquad \text{(VI.D.12)}$$

The $\widetilde{F}$, $\widetilde{G}$, and $\widetilde{FG}$ for a linear XYZ molecule in the gas phase are listed in Appendix F. Utilizing Eq. VI.A.3 the eigenvalues are

$$\lambda_2^g = f_2^g(\mu_X + \mu_Y) - f_{23}^g\mu_Y - f_2^g f_3^g \mu_Y^2/[f_3^g(\mu_Y + \mu_Z)$$
$$- f_2^g(\mu_X + \mu_Y)] \qquad \text{(VI.D.13)}$$

$$\lambda_3^g = f_3^g(\mu_Y + \mu_Z) - f_{23}^g\mu_Y - f_2^g f_3^g \mu_Y^2/[f_2^g(\mu_X + \mu_Y)$$
$$- f_3(\mu_Y + \mu_Z)] \qquad \text{(VI.D.14)}$$

Thus the matrix shifts for the stretching of the X-Y bond is

$$\lambda_2^g - \lambda_2^m = (f_2^g - f_2^m)(\mu_X + \mu_Y) + (f_{23}^m - f_{23}^g)\mu_Y$$
$$- f_1\mu_X^2/(\mu_X + \mu_Y) \qquad \text{(VI.D.15)}$$

where the small term on the right hand side of Eq. VI.D.8 and VI.D.9 are

are neglected. Likewise, the matrix shift for the stretching of the Y-Z bond is

$$\lambda_3^g - \lambda_3^m = (f_3^g - f_3^m)(\mu_Y + \mu_Z) + (f_{23}^m - f_{23}^g)\mu_Y - f_4\mu_Z^2/(\mu_Y + \mu_Z) \qquad \text{(VI.D.16)}$$

3. Triatomic molecules (bond bending modes)

Fig. VI.D.1c shows the model for the three doubly degenerate bending modes of a triatomic molecule in a rare gas cavity where M refers to the mass contribution of the cavity, X, Y, Z are the atoms in the triatomic molecule, r_1, r_4 are Van der Waals distances, r_2, r_3 are the gas phase equilibrium bond lengths, θ_1, θ_2, θ_3 are the coordinates for the bending modes, and, f_1, f_2, and f_3 are the bending force constants.

The $\widetilde{FG}$ elements for the three bending modes are listed in Appendix F where $H_{ij} = (FG)_{ij}$.

Utilizing Eq. VI.A.3 to find the eigenvalue for the bending mode of the XYZ molecule one obtains:

$$\lambda_2^m = f_2^m A - f_1 B^2/A - f_3 C^2/A \qquad \text{(VI.D.17)}$$

where

$$A = \mu_X/r_2^2 + \mu_Y(1/r_2 + 1/r_3)^2 + \mu_Z/r_3^2 \qquad \text{(VI.D.18)}$$

$$B = \mu_X(1/r_1 + 1/r_2)/r_2 + \mu_Y(1/r_2 + 1/r_3)/r_2 \qquad \text{(VI.D.19)}$$

$$C = \mu_Y(1/r_2 + 1/r_3)/r_3 + \mu_Z(1/r_3 + 1/r_4)/r_3 \qquad \text{(VI.D.20)}$$

The eigenvalue for the gas phase bending mode is

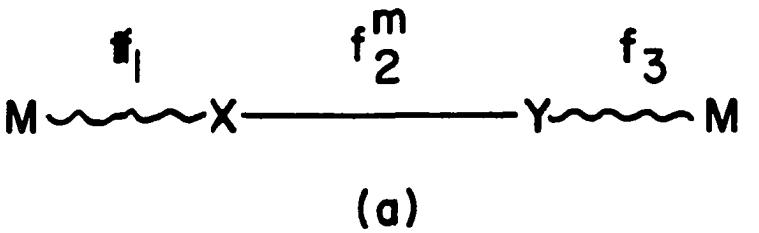

(a)

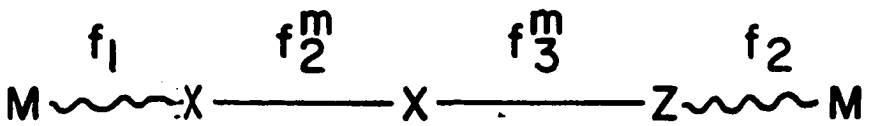

(b)

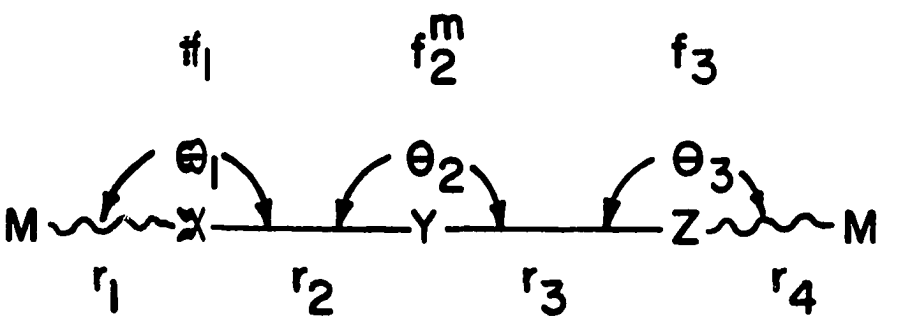

(c)

Fig. VI.D.1. Matrix models: (a) diatomic matrix model, (b) stretching modes for the triatomic matrix model, (c) bending modes for the triatomic matrix model

$$\lambda_2^g = f_2^g A \qquad \text{(VI.D.21)}$$

Thus the matrix shift for the bending mode is

$$\lambda_2^g - \lambda_2^m = (f_2^g - f_2^m)A - f_1 B^2/A - f_2 C^2/A \qquad \text{(VI.D.22)}$$

E. Matrix Elements for a Heteronuclear Diatomic in a Rare Gas Cavity

The $\widetilde{F}$, $\widetilde{G}$, and $\widetilde{H} = \widetilde{FG}$ matrix elements for a heteronuclear diatomic molecule in a rare gas cavity are:

$$F = \begin{vmatrix} f_1 & f_{12} & 0 \\ f_{12} & f_2^m & f_{23} \\ 0 & f_{23} & f_3 \end{vmatrix}$$

$$G = \begin{vmatrix} \mu_M + \mu_X & -\mu_X & 0 \\ -\mu_X & \mu_X + \mu_Y & -\mu_Y \\ 0 & -\mu_Y & \mu_Y + \mu_M \end{vmatrix}$$

$$H_{11} = f_1(\mu_M + \mu_X) - f_{12}\mu_X$$

$$H_{12} = f_{12}(\mu_X + \mu_Y) - f_1\mu_X$$

$$H_{13} = -f_{12}\mu_Y$$

$$H_{21} = f_{12}(\mu_M + \mu_X) - f_2^m\mu_X$$

$$H_{22} = f_2^m(\mu_X + \mu_Y) - \mu_X f_{12} - f_{23}\mu_Y$$

$$H_{23} = f_{23}(\mu_Y + \mu_M) - f_2^m \mu_Y$$

$$H_{31} = -\mu_X f_{23}$$

$$H_{32} = f_{23}(\mu_X + \mu_Y) - f_3 \mu_Y$$

$$H_{33} = f_3(\mu_Y + \mu_M) - f_{23} \mu_Y$$

F. $\widetilde{F}$, $\widetilde{G}$, and $\widetilde{H} = \widetilde{FG}$ Matrix Elements for the Stretching and Bending of a Linear Triatomic Molecule in a Rare Gas Cavity and in the Gas Phase

1. Stretching modes

The matrix elements for the stretching modes in a rare gas cavity are:

$$F = \begin{vmatrix} f_1 & f_{12} & 0 & 0 \\ f_{12} & f_2^m & f_{23}^m & 0 \\ 0 & f_{23}^m & f_3^m & f_{34} \\ 0 & 0 & f_{34} & f_4 \end{vmatrix}$$

$$G = \begin{vmatrix} \mu_M + \mu_H & -\mu_H & 0 & 0 \\ -\mu_H & \mu_H + \mu_C & -\mu_C & 0 \\ 0 & -\mu_C & \mu_C + \mu_N & -\mu_N \\ 0 & 0 & -\mu_N & \mu_N + \mu_M \end{vmatrix}$$

$$H_{11} = f_1(\mu_M + \mu_X) - f_{12} \mu_X$$

$$H_{12} = f_{12}(\mu_X + \mu_Y) - f_{11}\mu_X$$

$$H_{13} = - f_{12}\mu_Y$$

$$H_{14} = 0$$

$$H_{21} = f_{12}(\mu_M + \mu_X) - f_2\mu_X$$

$$H_{22} = f_2(\mu_X + \mu_Y) - f_{12}\mu_Y - f_{23}\mu_Y$$

$$H_{23} = f_{23}(\mu_Y + \mu_Z) - f_2\mu_Y$$

$$H_{24} = - f_{23}\mu_Z$$

$$H_{31} = - f_{23}\mu_Y$$

$$H_{32} = f_{23}(\mu_X + \mu_Y) - f_3\mu_Y$$

$$H_{33} = f_3(\mu_Y + \mu_Z) - \mu_Y f_{23} - \mu_Z f_{34}$$

$$H_{34} = f_{34}(\mu_Z + \mu_M) - \mu_Z f_3$$

$$H_{41} = 0$$

$$H_{42} = - f_{34}\mu_Y$$

$$H_{43} = f_{34}(\mu_Y + \mu_Z) - f_4\mu_Z$$

$$H_{44} = f_4(\mu_Y + \mu_Z) - f_{34}\mu_Z$$

The $\widetilde{F}$, $\widetilde{G}$, and $\widetilde{FG}$ for a linear triatomic molecule in the gas phase are:

$$F_{11} = f_2$$

$$F_{12} = f_{23}$$

$$F_{21} = f_{23}$$

$$F_{22} = f_3$$

$$G_{11} = \mu_X + \mu_Y$$

$$G_{12} = -\mu_X$$

$$G_{21} = -\mu_X$$

$$G_{22} = \mu_Y + \mu_Z$$

$$H_{11} = f_2(\mu_X + \mu_Y) - f_{23}\mu_Y$$

$$H_{12} = f_{23}(\mu_Y + \mu_Z) - f_3\mu_Y$$

$$H_{21} = f_{23}(\mu_X + \mu_Y) - f_2\mu_Y$$

$$H_{22} = f_3(\mu_Y + \mu_Z) - f_{23}\mu_Y$$

2. Bending modes

The $\tilde{H}$ matrix elements for the bending modes in a rare gas cavity are:

$$H_{11} = f_1[\mu_M/r_1^2 + \mu_X(1/r_1 + 1/r_2)^2 + \mu_Y/r_2^2]$$

$$- f_{12}[\mu_X(1/r_1 + 1/r_2)/r_2 + \mu_Y(1/r_2 + 1/r_3)/r_2] + f_{13}\mu_Y/r_2r_3$$

$$H_{12} = -f_1[\mu_X(1/r_1 + 1/r_2 + \mu_Y(1/r_2 + 1/r_3)/r_2]$$

$$+ f_{12}[\mu_X/r_2^2 + \mu_Y(1/r_2 + 1/r_3)^2 + \mu_Z/r_3^2$$

$$- f_{13}[\mu_Y(1/r_2 + 1/r_3)/r_3 + \mu_Z(1/r_3 + 1/r_4)/r_3]$$

$$H_{13} = - f_{12}[\mu_Y(1/r_2 + 1/r_3)/r_3 + \mu_Z(1/r_3 + 1/r_4)/r_3]$$

$$+ f_{13}[\mu_Y/r_3^2 + \mu_Z(1/r_3 + 1/r_4)^2 + \mu_M/r_4^2] + f_1\mu_Y/r_2r_3$$

$$H_{21} = f_{21}[\mu_M/r_1^2 + \mu_X(1/r_1 + 1/r_2)^2 + \mu_Y/r_2^2]$$

$$- f_2[\mu_X(1/r_1 + 1/r_2)/r_2 + \mu_Y(1/r_2 + 1/r_3)/r_2] + f_{23}\mu_Y/r_2r_3$$

$$H_{22} = - f_{12}[\mu_X(1/r_1 + 1/r_2)/r_2 + \mu_Y(1/r_2 + 1/r_3)/r_2]$$

$$+ f_2[\mu_X/r_2^2 + \mu_Y(1/r_2 + 1/r_3)^2 + \mu_Z/r_3^2]$$

$$- f_{23}[\mu_Y(1/r_2 + 1/r_3)/r_3 + \mu_Z(1/r_3 + 1/r_4)1/r_3]$$

$$H_{23} = - f_{12}[\mu_X(1/r_1 + 1/r_2)/r_2 + \mu_Y(1/r_2 + 1/r_3)/r_2]$$

$$- f_2[\mu_Y(1/r_2 + 1/r_3)/r_3 + \mu_Z(1/r_3 + 1/r_4)/r_3]$$

$$+ f_{23}[\mu_Y/r_3^2 + \mu_Z(1/r_3 + 1/r_4)^2 + \mu_M/r_4^2]$$

$$H_{31} = f_{13}[\mu_M/r_1^2 + \mu_X(1/r_1 + 1/r_2)^2 + \mu_Y/r_2^2]$$

$$- f_{23}[\mu_X(1/r_1 + 1/r_2)/r_2 + \mu_Y(1/r_2 + 1/r_3)/r_2] + f_3\mu_Y/r_2r_3$$

$$H_{32} = - f_{13}[\mu_X(1/r_1 + 1/r_2)/r_2 + \mu_Y(1/r_2 + 1/r_3)/r_2]$$

$$+ f_{23}[\mu_X/r_2^2 + \mu_Y(1/r_2 + 1/r_3)^2 + \mu_Z/r_3^2]$$

$$- f_3[\mu_Y(1/r_2 + 1/r_3)/r_3 + \mu_Z(1/r_3 + 1/r_4)/r_3]$$

$$H_{33} = - f_{23}[\mu_Y(1/r_2 + 1/r_3)/r_3 + \mu_Z(1/r_3 + 1/r_4)/r_3]$$

$$+ f_3[\mu_Y/r_3^2 + \mu_Z(1/r_3 + 1/r_4)^2 + \mu_M/r_4^2]$$

$$+ f_{13}\mu_Y/r_2r_3$$

The $\tilde{H}$ matrix element for the bending mode in the gas phase is

$$H_{22} = f_2[\mu_X/r_{XY}^2 + \mu_Z/r_{YZ}^2 + \mu_Y(1/r_{XY} + 1/r_{YZ})^2]$$

G. Measurement of the Band Center for ν_2 of $H^{12}C^{15}N$

The band center for ν_2 $H^{12}C^{15}N$ has not been reported in the literature. The measurement of this band center is reported in this section.

The $H^{12}C^{15}N$ was prepared from 98% ^{15}N enriched $K^{12}C^{15}N$ by the method given in Section III.A. The $H^{12}C^{15}N$ gas was contained in a cell with a 20 cm path length filled to a pressure of approximately one mm Hg. The spectral slit widths were approximately 0.15 cm^{-1}. The spectra were calibrated against gas phase $H^{12}C^{14}N$ spectra (34).

The first two columns in Table VI.G.1 shows the results of two calculations for the bands measured in the P and R branches. The average of the two calibrations was used in the following expression to find the band center:

$$\nu_2(H^{12}C^{15}N) = [R(J-1) + P(J)]/2$$

The band center for the bending vibration of $H^{12}C^{15}N$, ν_2 = 711.02 ± 0.03.

Table VI.G.1. Calibration of ν_2 $H^{12}C^{15}N$ in the gas phase

	Run 1	Run 2	Average	$[R(J-1) + P(J)]/_2$
R(5)	728.25	728.23	728.24	
R(4)	725.37	725.34	725.36	
R(3)	722.54	722.54	722.54	
R(2)	719.63	719.60	719.62	
R(1)	716.80	716.77	716.78	
				711.02 ± 0.03
P(2)	705.24	705.31	705.24	
P(3)	702.40	702.39	702.40	
P(4)	699.51	699.52	699.52	
P(5)	696.66	696.71	696.69	
P(6)	693.75	693.76	693.76	

H. Band Intensity Measurements for ν_2 and ν_3 of $H^{12}C^{14}N$ and $H^{13}C^{14}N$ in an Argon Matrix

The HCN samples were prepared by the method given in Section III.A. The KCN sample was stated by the manufacturer to contain 57% C^{13}. However, subsequent analysis by mass spectrometry showed the sample to contain 50% C^{13}.

The spectra were all recorded under identical conditions except that a thicker matrix was used to record the ν_3 band.

After the spectra were transformed from a transmittance to an absorbance scale the bands were integrated with a planimeter. Table VI.H.1 summarizes the results where the first four columns are the areas obtained in arbitrary units for two different runs. The last column contains the ratio A'/A which is the relative intensity of ν_2 or ν_3 for $H^{13}C^{14}N$ to $H^{12}C^{14}N$. The ratios A'/A agree within experimental error and show that the band intensities for both ν_2 and ν_3 for $H^{13}C^{14}N$ are more intense than those for $H^{12}C^{14}N$.